Interaction Notes

Note 528

July 1, 1997

CLEARED
FOR PUBLIC RELEASE
PL/PA 22AUG97

Asymptotic Analysis of the Natural System Modes of Coupled Bodies in the Large Separation, Low-Frequency Regime

George W. Hanson
University of Wisconsin-Milwaukee

Carl E. Baum
Phillips Laboratory

Abstract

In this note we examine the natural system modes (characteristic frequencies and currents) of two coupled bodies in the limit of large separation. It is known that when objects are situated such that they may interact electromagnetically, natural modes of the coupled system occur. These modes differ from the natural modes of the isolated bodies, but may be related to the isolated body modes for some situations. For example, for two identical bodies separated by some intermediate distance, the first antisymmetric and symmetric system frequencies spiral around the dominant natural frequency of the isolated body as separation is varied. As separation further increases, these system resonances tend towards the origin in the complex frequency plane, rather than approaching the isolated-body dominant natural frequency. Here we treat an N-body scattering problem in the limit of large separation by replacing the bodies with equivalent dipole moments. The natural frequencies are obtained as singular points in the scattering solution. For the special case of two coupled objects, a simple equation for the natural system frequencies is obtained which shows that the real radian system frequency approaches the origin as $1/r$, independent of the relative orientation and type of the two bodies. The damping coefficient approaches the origin approximately logarithmically, as a function of the body orientation and type. This simple equation leads to classification and ordering of some system modes based on their behavior in the limit of large separation. Using this formulation, the natural system modes of two coupled wires are investigated for large separation between the wires, and compared to an integral equation solution. For completeness, results from the integral equation solution of the two-wire problem are provided for small wire separation, to show the evolution of the modes obtained from the asymptotic formulation beyond its range of validity.

PL 97-1081

DEPARTMENT OF THE AIR FORCE
PHILLIPS LABORATORY (AFMC)

Date: 3 SEP 97

MEMORANDUM FOR PL/WSQW

ATTENTION: Dr. Carl E. Baum

FROM: PL/PA

SUBJECT: Phillips Laboratory Security Review Case Number(s) PL 97-1077, 1080 & 1081

1. Action on the security review case mentioned above has been completed with the following determination, as marked:

X **CLEARED FOR OPEN PUBLICATION/PRESENTATION (NO CHANGES.)**

___ **CLEARED FOR OPEN PUBLICATION/PRESENTATION AS AMENDED**. The amendments, changes, deletions, etc., denoted by the words "as amended? -- are mandatory. Words of information to be deleted are indicated inside brackets.

___ **CLEARED FOR OPEN PUBLICATION/PRESENTATION WITH RECOMMENDED CHANGES.** The reviewers have suggested some changes which are not mandatory, indicated by the words "recommended changes."

___ **DISAPPROVED FOR PUBLIC RELEASE** for the following reason(s)

___ **Contained Classified Information**

___ **Contained Technology Security Information Determined Not to be releasable to the public**

___ **Release Denied for other AF/DoD/Government reasons**

X **The PL project officer must notify the author/contractor about the decision on this case and send them a copy of this letter with a copy of the stamped document (attached).**

___ **OTHER**: _____

_____.

If you have questions, please call me at (505) 846-6246.

JUDY L. JOHNSTON
Security Review Officer

Attachments:
1. PL 97-1077
2. PL 97-1080
3. PL 97-1081

printed on recycled paper.

Interaction Notes

Note 528

July 1, 1997

Asymptotic Analysis of the Natural System Modes of Coupled Bodies in the Large Separation, Low-Frequency Regime

George W. Hanson
University of Wisconsin-Milwaukee

Carl E. Baum
Phillips Laboratory

Abstract

In this note we examine the natural system modes (characteristic frequencies and currents) of two coupled bodies in the limit of large separation. It is known that when objects are situated such that they may interact electromagnetically, natural modes of the coupled system occur. These modes differ from the natural modes of the isolated bodies, but may be related to the isolated body modes for some situations. For example, for two identical bodies separated by some intermediate distance, the first antisymmetric and symmetric system frequencies spiral around the dominant natural frequency of the isolated body as separation is varied. As separation further increases, these system resonances tend towards the origin in the complex frequency plane, rather than approaching the isolated-body dominant natural frequency. Here we treat an N-body scattering problem in the limit of large separation by replacing the bodies with equivalent dipole moments. The natural frequencies are obtained as singular points in the scattering solution. For the special case of two coupled objects, a simple equation for the natural system frequencies is obtained which shows that the real radian system frequency approaches the origin as $1/r$, independent of the relative orientation and type of the two bodies. The damping coefficient approaches the origin approximately logarithmically, as a function of the body orientation and type. This simple equation leads to classification and ordering of some system modes based on their behavior in the limit of large separation. Using this formulation, the natural system modes of two coupled wires are investigated for large separation between the wires, and compared to an integral equation solution. For completeness, results from the integral equation solution of the two-wire problem are provided for small wire separation, to show the evolution of the modes obtained from the asymptotic formulation beyond its range of validity.

I. Introduction

The electromagnetic response of coupled bodies is of interest in many applications, including target detection and identification. In this note we consider the frequency (s-plane) behavior of the system resonances of coupled objects in the limit of large separation.

In an early paper relating to the singularity expansion method (SEM) it was observed that the SEM frequencies of an isolated thin wire scatterer can be grouped in layers in the s-plane nearly parallel to the $j\omega$ axis [1]. These resonances are further identified by their position within these layers. This observation naturally leads to the notation for the complex frequencies $s_{n,l}^{0}$, where n denotes the nth pole as measured from the Re(s) axis in the lth layer, measured from the $j\omega$ axis. Similar groupings can be identified for other objects, but to illustrate the effect considered here the situation for thin wires will be described.

Shortly after the above observations were made concerning isolated wires, the natural system frequencies of coupled wires were studied. It was found that these system resonances exhibited some interesting characteristics as wire separation was varied [2]. To simplify the discussion, consider two identical wires, for which the system resonances can be divided into symmetric ($s_{n,l}^{s}$) and antisymmetric ($s_{n,l}^{a}$) modes [14]. As observed in [2] for two thin wire scatterers, the low-order system resonances ($s_{1,1}^{a,s}$) tended to spiral around the dominant isolated body resonance ($s_{1,1}^{0}$) as spacing between the objects was varied over some intermediate distance. As separation was further increased, the system resonances moved off towards the origin in the complex frequency plane, and other system modes from another layer moved in to take their place, again spiraling around $s_{1,1}^{0}$. Subsequent to [2], other papers further considered coupled wire scatterers [3]-[4].

The fact that the system frequencies eventually tended towards the origin as spacing is increased beyond some intermediate distance, rather than tending towards the isolated body resonances, was discussed in [2], and explained from a time-domain perspective in [5]. It was observed that the SEM system modes are global quantities for the coupled body system, and have no clear physical interpretation prior to times when global modes can be established. Hence, in a two-body system the time period after which the scattered field from each body has interacted with the other body is designated as late time. During late time, the two objects interact electromagnetically, and global system modes are established. As spacing between the objects becomes large relative to the largest linear dimension of each body, the system resonances tend towards low frequencies since the time for a wave to travel between the two bodies becomes long. Eventually the spacing tends towards infinity, and the system resonances tend toward zero.

Since the resonances of a coupled system are rigorously obtained from a complicated (usually integral) system of equations, simple approximate formulas which describe the system resonance behavior as a function of body separation are of interest. For intermediate separations, perturbation formulas have been obtained which relate the natural system frequencies to the natural frequencies of the isolated bodies. Two related classes of perturbation solution have been obtained, both based upon the exact integral-operator description of the coupled system. The first method yields a quasi-analytic formula for the system frequencies of an object and a mirror object, separated by some intermediate distance. The resulting formula involves a numerically computed coefficient which only depends upon the isolated object's characteristics, multiplied by an exponential term which is a function of the separation between the objects [6]. The second method is more numerical in nature, yet represents a considerable simplification of the exact IEs and is applicable to a more general system of coupled bodies [7]. The formulation described in [7] was subsequently applied to a variety of coupled objects [5], [8]-[9].

In this note, we present a scattering formulation for N coupled objects valid in the limit of large

separation between all objects. The system of scatterers are replaced by interacting dipole moments, which is a suitable approximation for large separations (which lead to low system frequencies). A simpler formulation is provided for two objects coupled in a mirror symmetric configuration. Singularities of the scattering solution are identified as natural frequencies, leading to the characteristic equation for natural frequencies of the coupled system. The example of two coupled wires is considered to demonstrate the accuracy of the asymptotic method, where the natural system frequencies from the asymptotic formulation are compared to those generated from a full-wave integral equation solution. The system modes are classified according to their behavior for large separation between the bodies, and some results for the natural currents are provided to examine their behavior in the corresponding limit.

II. Preliminary Relations

Consider Maxwell's curl equations for free space in the two-sided Laplace transform domain

$$\begin{aligned} \nabla\times\vec{E}(\vec{r},s) &= -s\vec{B}(\vec{r},s) - \vec{J}^{m}(\vec{r},s) \\ \nabla\times\vec{H}(\vec{r},s) &= s\vec{D}(\vec{r},s) + \vec{J}^{e}(\vec{r},s)\,. \end{aligned} \tag{1}$$

The relationships between fields and currents are given in terms of four Green's dyadics as [10]

$$\begin{aligned} \vec{E}(\vec{r},s) &= -s\mu_0\left\langle \ddot{G}_{e,e}(\vec{r}|\vec{r}',s)\,;\vec{J}^{e}(\vec{r}',s)\right\rangle \\ &\quad +\left\langle \ddot{G}_{e,m}(\vec{r}|\vec{r}',s)\,;\vec{J}^{m}(\vec{r}',s)\right\rangle \\ \vec{H}(\vec{r},s) &= -s\epsilon_0\left\langle \ddot{G}_{h,m}(\vec{r}|\vec{r}',s)\,;\vec{J}^{m}(\vec{r}',s)\right\rangle \\ &\quad +\left\langle \ddot{G}_{h,e}(\vec{r}|\vec{r}',s)\,;\vec{J}^{e}(\vec{r}',s)\right\rangle \end{aligned} \tag{2}$$

where the bracket notation indicates a real inner product with integration over common spatial coordinates (typically volume or surface integration). The Green's dyadics are

$$\ddot{G}_{e,e}(\vec{r}|\vec{r}',s) = PV\left[\ddot{1}-\gamma^{-2}\nabla\nabla\right]G(\vec{r}|\vec{r}',s) + \gamma^{-2}\ddot{L}(\vec{r})\,\delta(\vec{r}-\vec{r}') \tag{3}$$

$$\ddot{G}_{e,m}(\vec{r}|\vec{r}',s) = -\nabla G(\vec{r}|\vec{r}',s)\times\ddot{1} \tag{4}$$

$$\ddot{G}_{h,e}(\vec{r}|\vec{r}',s) = -\ddot{G}_{e,m}(\vec{r}|\vec{r}',s) \tag{5}$$

$$\ddot{G}_{h,m}(\vec{r}|\vec{r}',s) = \ddot{G}_{e,e}(\vec{r}|\vec{r}',s) \tag{6}$$

where $G(\vec{r}|\vec{r}',s) = \dfrac{\gamma e^{-\xi}}{4\pi\xi}$ is the free-space scaler Green's function, with $\gamma = \dfrac{s}{c}$, $\xi = \gamma R$, $c = (\epsilon_0\mu_0)^{-1/2}$, and $R = |\vec{r}-\vec{r}'|$. The first term in (3) can be written as

$$[\bar{\bar{1}} - \gamma^{-2}\nabla\nabla]G(\vec{r}|\vec{r}', s) = \frac{\gamma e^{-\xi}}{4\pi}\{[-2\xi^{-3} - 2\xi^{-2}]\,\vec{1}_R\vec{1}_R + [\xi^{-3} + \xi^{-2} + \xi^{-1}][\bar{\bar{1}} - \vec{1}_R\vec{1}_R]\} \quad (7)$$

$$= -\frac{\gamma e^{-\xi}}{4\pi}\{[3\vec{1}_R\vec{1}_R - \bar{\bar{1}}](\xi^{-3} + \xi^{-2}) + [\vec{1}_R\vec{1}_R - \bar{\bar{1}}]\xi^{-1}\}$$

where $\vec{1}_R = \dfrac{\vec{r} - \vec{r}'}{|\vec{r} - \vec{r}'|}$, and $\bar{\bar{1}} = \vec{1}_x\vec{1}_x + \vec{1}_y\vec{1}_y + \vec{1}_z\vec{1}_z$ is the identity dyadic. For later convenience, define

$$\bar{\bar{F}}_{e,e}(\vec{r}|\vec{r}', s) \equiv \frac{e^{-\gamma R}}{4\pi}\left\{[3\vec{1}_R\vec{1}_R - \bar{\bar{1}}]\left(\frac{1}{\epsilon_0 R^3} + \frac{sZ_0}{R^2}\right) + [\vec{1}_R\vec{1}_R - \bar{\bar{1}}]\,\frac{s^2\mu_0}{R}\right\} \quad (8)$$

with $Z_0 = \sqrt{\dfrac{\mu_0}{\epsilon_0}}$, such that the $\bar{\bar{G}}_{e,e}$ term can be expressed as

$$\bar{\bar{G}}_{e,e}(\vec{r}|\vec{r}', s) = PV\frac{-1}{s^2\mu_0}\bar{\bar{F}}_{e,e}(\vec{r}|\vec{r}', s) + \gamma^{-2}\vec{L}(\vec{r})\,\delta(\vec{r} - \vec{r}')\,. \quad (9)$$

The magnetic Green's dyadic, $\bar{\bar{G}}_{e,m}$, can be expressed as

$$\bar{\bar{G}}_{e,m}(\vec{r}|\vec{r}', s) = -\nabla G(\vec{r}|\vec{r}', s) \times \bar{\bar{1}} = \frac{e^{-\gamma R}}{4\pi}\left[\frac{1}{R^2} + \frac{s}{Rc}\right]\vec{1}_R \times \bar{\bar{1}} \quad (10)$$

where upon defining for later convenience

$$F_{e,m}(\vec{r}|\vec{r}', s) \equiv \frac{e^{-\gamma R}}{4\pi}\left(\frac{s\mu_0}{R^2} + \frac{s^2\mu_0}{Rc}\right) \quad (11)$$

the magnetic Green's dyadic can be written as

$$\bar{\bar{G}}_{e,m}(\vec{r}|\vec{r}', s) = \frac{1}{s\mu_0}F_{e,m}(\vec{r}|\vec{r}', s)\,\vec{1}_R \times \bar{\bar{1}}\,. \quad (12)$$

In (3), the PV notation indicates that the corresponding term should be integrated in the principal value sense [10], where

$$\vec{L}(\vec{r}) = \frac{1}{4\pi}\int_{S_\delta}\frac{\vec{1}_S(\vec{r}')\,\vec{1}_{R'}(\vec{r}|\vec{r}')}{|\vec{r} - \vec{r}'|^2}\,dS' \quad (13)$$

is the depolarizing dyadic integral, evaluated over the surface S_δ of the exclusion volume V_δ excluded in the PV integration. In (13), $\vec{1}_{R'}(\vec{r}|\vec{r}') = -\vec{1}_R(\vec{r}|\vec{r}') = \vec{1}_R(\vec{r}'|\vec{r})$, and $\vec{1}_S(\vec{r})$ is the unit normal vector to S at $\vec{r}$. Note that the $\bar{\bar{G}}_{\{h,m\}}^{\{e,e\}}$ terms are properly interpreted as distributions.

III. Scattering formulation

Consider a N-body scattering problem which can be analyzed by formulating a coupled set of integral equations for the current (surface or volume polarization) induced on/in the objects by an incident field. When the separation between all objects becomes large compared to the largest linear dimension of each object, and in the limit of low frequency, the formulation can be considerably simplified by replacing each object with equivalent dipole moments. This follows from the fact that the electric and magnetic dipole moment terms dominant the fields due to a given current (as in a multipole expansion of the current) for large distances and low frequencies [12]. To formulate the desired set of equations, the scatterers, which are assumed to reside in free space, are replaced with dipole moments $\vec{p}^{\beta}$, $\vec{m}^{\beta}$ for $\beta = 1, 2, \ldots, N$ corresponding to object 1,2,...N, respectively, as shown in Fig. 1. The dipoles are considered to be generated by fields via polarizability dyadics as

$$\begin{aligned} \vec{p}^{(\beta)}(s) &= \epsilon_0 \ddot{P}^{(\beta)}(s) \cdot \vec{E}(\vec{r}_\beta, s) \\ \vec{m}^{(\beta)}(s) &= \ddot{M}^{(\beta)}(s) \cdot \vec{H}(\vec{r}_\beta, s) \end{aligned} \tag{14}$$

where the fields $(\vec{E}, \vec{H})$ are the total fields due to all dipoles not located at $\vec{r}_\beta$, plus any externally impressed field. The polarizability dyadics are symmetrical for reciprocal media,

$$\begin{aligned} \ddot{P}^{(\beta)T}(s) &= \ddot{P}^{(\beta)}(s) \\ \ddot{M}^{(\beta)T}(s) &= \ddot{M}^{(\beta)}(s) \end{aligned} \tag{15}$$

and as $s \to 0$ [12]

$$\begin{aligned} \ddot{P}^{(\beta)}(s) &= \ddot{P}_0^{(\beta)} + O(s) \\ \ddot{M}^{(\beta)}(s) &= \ddot{M}_0^{(\beta)} + O(s) . \end{aligned} \tag{16}$$

The currents associated with the dipole moments are

$$\begin{aligned} \vec{J}_e^{(\beta)} &= s\vec{p}^{(\beta)} \delta(\vec{r} - \vec{r}_\beta) \\ \vec{J}_m^{(\beta)} &= s\mu_0 \vec{m}^{(\beta)} \delta(\vec{r} - \vec{r}_\beta) . \end{aligned} \tag{17}$$

Inserting (17) into (2) leads to the fields at $\vec{r}_\alpha$ maintained by electric and magnetic dipoles located at $\vec{r}_\beta$ as

$$\begin{aligned} \vec{E}^{(\alpha,\beta)}(\vec{r}_\alpha, s) &= \ddot{F}_{e,e}(\vec{r}_\alpha | \vec{r}_\beta, s) \cdot \vec{p}^{(\beta)}(s) + F_{e,m}(\vec{r}_\alpha | \vec{r}_\beta, s) \left(\vec{1}_{R_{\alpha,\beta}} \times \vec{1}\right) \cdot \vec{m}^{(\beta)}(s) \\ \vec{H}^{(\alpha,\beta)}(\vec{r}_\alpha, s) &= -\frac{1}{\mu_0} F_{e,m}(\vec{r}_\alpha | \vec{r}_\beta, s) \left(\vec{1}_{R_{\alpha,\beta}} \times \vec{1}\right) \cdot \vec{p}^{(\beta)}(s) + \epsilon_0 \ddot{F}_{e,e}(\vec{r}_\alpha | \vec{r}_\beta, s) \cdot \vec{m}^{(\beta)}(s) \end{aligned} \tag{18}$$

where

$$\vec{\vec{F}}_{e,e}(\vec{r}_\alpha|\vec{r}_\beta, s) = \frac{e^{-\gamma R_{\alpha,\beta}}}{4\pi}\left\{\left[3\vec{1}_{R_{\alpha,\beta}}\vec{1}_{R_{\alpha,\beta}} - \vec{\vec{1}}\right]\left(\frac{1}{\epsilon_0 R_{\alpha,\beta}^3} + \frac{sZ_0}{R_{\alpha,\beta}^2}\right) + \left[\vec{1}_{R_{\alpha,\beta}}\vec{1}_{R_{\alpha,\beta}} - \vec{\vec{1}}\right]\frac{s^2\mu_0}{R_{\alpha,\beta}}\right\}$$

$$F_{e,m}(\vec{r}_\alpha|\vec{r}_\beta, s) = \frac{e^{-\gamma R_{\alpha,\beta}}}{4\pi}\left\{\frac{\mu_0 s}{R_{\alpha,\beta}^2} + \frac{\mu_0 s^2}{R_{\alpha,\beta} C}\right\} \qquad (19)$$

with $\vec{1}_{R_{\alpha,\beta}} = \frac{\vec{r}_\alpha - \vec{r}_\beta}{|\vec{r}_\alpha - \vec{r}_\beta|}$ being the unit vector from $\vec{r}_\beta$ to $\vec{r}_\alpha$, and $R_{\alpha,\beta} = |\vec{r}_\alpha - \vec{r}_\beta|$. The total field at $\vec{r}_\alpha$ due to N-1 dipoles located at $\vec{r}_\beta$, $\beta = 1, 2, \ldots N$, $\beta \neq \alpha$ is

$$\vec{E}(\vec{r}_\alpha, s) = \sum_{\substack{\beta=1 \\ \beta\neq\alpha}}^{N} \vec{E}^{(\alpha,\beta)}(\vec{r}_\alpha, s)$$

$$\vec{H}(\vec{r}_\alpha, s) = \sum_{\substack{\beta=1 \\ \beta\neq\alpha}}^{N} \vec{H}^{(\alpha,\beta)}(\vec{r}_\alpha, s)\,. \qquad (20)$$

Considering the scatterers to be as shown in Fig. 1, a coupled system of equations for the induced dipole moments can be written down as

$$\vec{p}^{(\alpha)}(s) = \epsilon_0 \vec{\vec{P}}_0^{(\alpha)} \cdot \left[\vec{E}^{(inc)}(\vec{r}_\alpha, s) + \sum_{\substack{\beta=1 \\ \beta\neq\alpha}}^{N} \vec{E}^{(\alpha,\beta)}(\vec{r}_\alpha, s)\right]$$

$$\vec{m}^{(\alpha)}(s) = \vec{\vec{M}}_0^{(\alpha)} \cdot \left[\vec{H}^{(inc)}(\vec{r}_\alpha, s) + \sum_{\substack{\beta=1 \\ \beta\neq\alpha}}^{N} \vec{H}^{(\alpha,\beta)}(\vec{r}_\alpha, s)\right] \qquad (21)$$

$$\alpha = 1, 2, \ldots, N$$

where the fields $(\vec{E}^{(inc)}, \vec{H}^{(inc)})$ are externally impressed fields. Defining

$$\vec{\vec{F}}_{e,e}^{(\alpha,\beta)} \equiv \vec{\vec{F}}_{e,e}(\vec{r}_\alpha|\vec{r}_\beta, s)$$

$$F_{e,m}^{(\alpha,\beta)} \equiv F_{e,m}(\vec{r}_\alpha|\vec{r}_\beta, s) = F_{e,m}(\vec{r}_\beta|\vec{r}_\alpha, s) \qquad (22)$$

the set of equations (21) can be written as

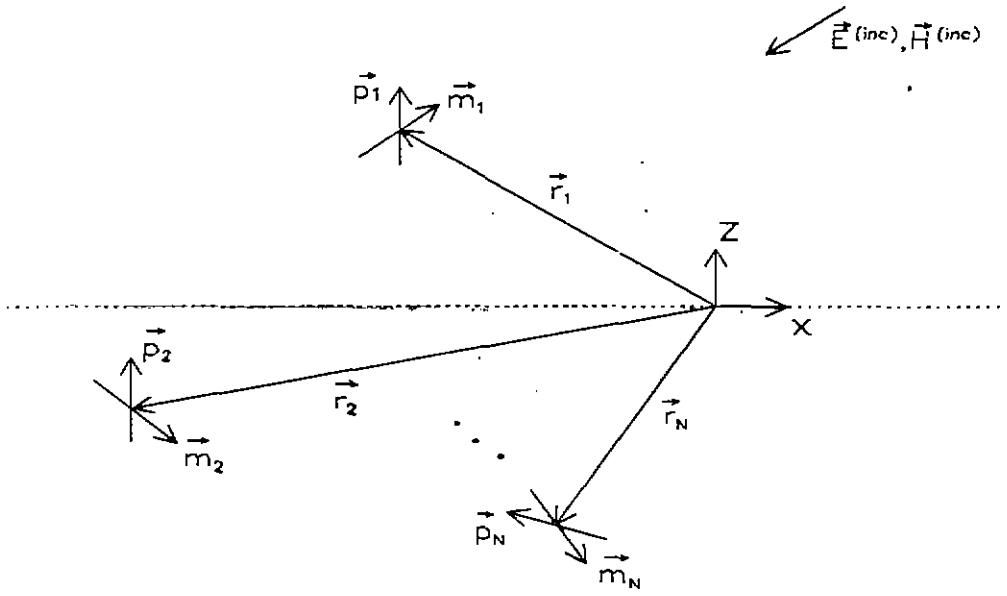

Fig. 1. Configuration of N interacting dipoles.

$$\vec{p}^{(\alpha)}(s) - \epsilon_0 \ddot{P}_0^{(\alpha)} \cdot \sum_{\substack{\beta=1 \\ \beta \neq \alpha}}^{N} \left[\ddot{F}_{e,e}^{(\alpha,\beta)} \cdot \vec{p}^{(\beta)} + F_{e,m}^{(\alpha,\beta)} \left(\vec{1}_{R_{\alpha,\beta}} \times \ddot{1} \right) \cdot \vec{m}^{(\beta)} \right] = \epsilon_0 \ddot{P}_0^{(\alpha)} \cdot \vec{E}^{(inc)}(\vec{r}_\alpha, s)$$

$$\vec{m}^{(\alpha)}(s) - \ddot{M}_0^{(\alpha)} \cdot \sum_{\substack{\beta=1 \\ \beta \neq \alpha}} \left[-\frac{1}{\mu_0} F_{e,m}^{(\alpha,\beta)} \left(\vec{1}_{R_{\alpha,\beta}} \times \ddot{1} \right) \cdot \vec{p}^{(\beta)} + \epsilon_0 \ddot{F}_{e,e}^{(\alpha,\beta)} \cdot \vec{m}^{(\beta)} \right] = \ddot{M}_0^{(\alpha)} \cdot \vec{H}^{(inc)}(\vec{r}_\alpha, s)$$

$$\alpha = 1, 2, \ldots, N \qquad (23)$$

It is convenient to write the above in block dyadic form

$$\begin{bmatrix} \ddot{I}_{2\times2} & \ddot{Q}_{2\times2}^{(1,2)}(s) & \ddot{Q}_{2\times2}^{(1,3)}(s) & \cdots & \ddot{Q}_{2\times2}^{(1,N)}(s) \\ \ddot{Q}_{2\times2}^{(2,1)}(s) & \ddot{I}_{2\times2} & \ddot{Q}_{2\times2}^{(2,3)}(s) & \cdots & \ddot{Q}_{2\times2}^{(2,N)}(s) \\ \ddot{Q}_{2\times2}^{(3,1)}(s) & \ddot{Q}_{2\times2}^{(3,2)}(s) & \ddot{I}_{2\times2} & \cdots & \ddot{Q}_{2\times2}^{(3,N)}(s) \\ \vdots & \vdots & \vdots & \vdots & \vdots \\ \ddot{Q}_{2\times2}^{(N,1)}(s) & \ddot{Q}_{2\times2}^{(N,2)}(s) & \ddot{Q}_{2\times2}^{(N,3)}(s) & \cdots & \ddot{I}_{2\times2} \end{bmatrix} \cdot \begin{bmatrix} \vec{d}_{2\times1}^{(1)}(s) \\ \vec{d}_{2\times1}^{(2)}(s) \\ \vec{d}_{2\times1}^{(3)}(s) \\ \vdots \\ \vec{d}_{2\times1}^{(N)}(s) \end{bmatrix} = \begin{bmatrix} \vec{F}_{2\times1}^{(1)}(s) \\ \vec{F}_{2\times1}^{(2)}(s) \\ \vec{F}_{2\times1}^{(3)}(s) \\ \vdots \\ \vec{F}_{2\times1}^{(N)}(s) \end{bmatrix} \tag{24}$$

where

$$\ddot{Q}_{2\times2}^{(\alpha,\beta)}(s) \equiv \begin{bmatrix} -\epsilon_0 \ddot{P}_0^{(\alpha)} \cdot \ddot{F}_{e,e}^{(\alpha,\beta)} & -\epsilon_0 F_{e,m}^{(\alpha,\beta)} \ddot{P}_0^{(\alpha)} \cdot \left(\vec{1}_{R_{\alpha,\beta}} \times \ddot{I}\right) \\ \frac{1}{\mu_0} F_{e,m}^{(\alpha,\beta)} \ddot{M}_0^{(\alpha)} \cdot \left(\vec{1}_{R_{\alpha,\beta}} \times \ddot{I}\right) & -\epsilon_0 \ddot{M}_0^{(\alpha)} \cdot \ddot{F}_{e,e}^{(\alpha,\beta)} \end{bmatrix} \tag{25}$$

$$\ddot{I}_{2\times2} \equiv \begin{bmatrix} \ddot{I} & \ddot{0} \\ \ddot{0} & \ddot{I} \end{bmatrix}, \quad \vec{d}_{2\times1}^{(\alpha)}(s) \equiv \begin{bmatrix} \vec{p}^{(\alpha)}(s) \\ \vec{m}^{(\alpha)}(s) \end{bmatrix}, \quad \vec{F}_{2\times1}^{(\alpha)}(s) \equiv \begin{bmatrix} \epsilon_0 \ddot{P}_0^{(\alpha)} \cdot \vec{E}^{(inc)}(\vec{r}_\alpha, s) \\ \ddot{M}_0^{(\alpha)} \cdot \vec{H}^{(inc)}(\vec{r}_\alpha, s) \end{bmatrix}. \tag{26}$$

Providing that the left-hand dyadic matrix is non-singular, (24) can be inverted to yield

$$\begin{bmatrix} \vec{d}_{2\times1}^{(1)}(s) \\ \vec{d}_{2\times1}^{(2)}(s) \\ \vec{d}_{2\times1}^{(3)}(s) \\ \vdots \\ \vec{d}_{2\times1}^{(N)}(s) \end{bmatrix} = \begin{bmatrix} \ddot{I}_{2\times2} & \ddot{Q}_{2\times2}^{(1,2)}(s) & \ddot{Q}_{2\times2}^{(1,3)}(s) & \cdots & \ddot{Q}_{2\times2}^{(1,N)}(s) \\ \ddot{Q}_{2\times2}^{(2,1)}(s) & \ddot{I}_{2\times2} & \ddot{Q}_{2\times2}^{(2,3)}(s) & \cdots & \ddot{Q}_{2\times2}^{(2,N)}(s) \\ \ddot{Q}_{2\times2}^{(3,1)}(s) & \ddot{Q}_{2\times2}^{(3,2)}(s) & \ddot{I}_{2\times2} & \cdots & \ddot{Q}_{2\times2}^{(3,N)}(s) \\ \vdots & \vdots & \vdots & \vdots & \vdots \\ \ddot{Q}_{2\times2}^{(N,1)}(s) & \ddot{Q}_{2\times2}^{(N,2)}(s) & \ddot{Q}_{2\times2}^{(N,3)}(s) & \cdots & \ddot{I}_{2\times2} \end{bmatrix}^{-1} \cdot \begin{bmatrix} \vec{F}_{2\times1}^{(1)}(s) \\ \vec{F}_{2\times1}^{(2)}(s) \\ \vec{F}_{2\times1}^{(3)}(s) \\ \vdots \\ \vec{F}_{2\times1}^{(N)}(s) \end{bmatrix} \tag{27}$$

Equation (27) provides a formal solution to the scattering problem for configurations and frequencies such that the dipole moment approximation is valid. Scattered fields are obtained by substituting (27) into (20).

Each dyadic block, with the exception of the identity blocks, is a function of complex frequency s. In this note we are primarily interested in determining the natural frequencies such that the left-hand block-dyadic matrix is singular. At a natural frequency,

$$\det \begin{bmatrix} \ddot{I}_{2\times2} & \ddot{Q}_{2\times2}^{(1,2)}(s) & \ddot{Q}_{2\times2}^{(1,3)}(s) & \cdots & \ddot{Q}_{2\times2}^{(1,N)}(s) \\ \ddot{Q}_{2\times2}^{(2,1)}(s) & \ddot{I}_{2\times2} & \ddot{Q}_{2\times2}^{(2,3)}(s) & \cdots & \ddot{Q}_{2\times2}^{(2,N)}(s) \\ \ddot{Q}_{2\times2}^{(3,1)}(s) & \ddot{Q}_{2\times2}^{(3,2)}(s) & \ddot{I}_{2\times2} & \cdots & \ddot{Q}_{2\times2}^{(3,N)}(s) \\ \vdots & \vdots & \vdots & \vdots & \vdots \\ \ddot{Q}_{2\times2}^{(N,1)}(s) & \ddot{Q}_{2\times2}^{(N,2)}(s) & \ddot{Q}_{2\times2}^{(N,3)}(s) & \cdots & \ddot{I}_{2\times2} \end{bmatrix} = 0 \tag{28}$$

which forms the fundamental characteristic equation for natural system frequencies of N interacting

objects in the large separation, low frequency regime.

For the special case of two interacting dipoles,

$$\begin{bmatrix} \vec{d}_{2\times1}^{(1)}(s) \\ \vec{d}_{2\times1}^{(2)}(s) \end{bmatrix} = \begin{bmatrix} \vec{\mathrm{I}}_{2\times2} & \vec{Q}_{2\times2}^{(1,2)}(s) \\ \vec{Q}_{2\times2}^{(2,1)}(s) & \vec{\mathrm{I}}_{2\times2} \end{bmatrix}^{-1} \cdot \begin{bmatrix} \vec{F}_{2\times1}^{(1)}(s) \\ \vec{F}_{2\times1}^{(2)}(s) \end{bmatrix} \tag{29}$$

where [13]

$$\begin{bmatrix} \vec{\mathrm{I}}_{2\times2} & \vec{Q}_{2\times2}^{(1,2)} \\ \vec{Q}_{2\times2}^{(2,1)} & \vec{\mathrm{I}}_{2\times2} \end{bmatrix}^{-1} = \begin{bmatrix} \vec{A}_{2\times2} & \vec{B}_{2\times2} \\ \vec{C}_{2\times2} & \vec{D}_{2\times2} \end{bmatrix} \tag{30}$$

with

$$\begin{aligned} \vec{A}_{2\times2} &= \left[\vec{\mathrm{I}}_{2\times2} - \vec{Q}_{2\times2}^{(1,2)} \cdot \vec{\mathrm{I}}_{2\times2}^{-1} \cdot \vec{Q}_{2\times2}^{(2,1)}\right]^{-1} \\ \vec{B}_{2\times2} &= -\left[\vec{\mathrm{I}}_{2\times2} - \vec{Q}_{2\times2}^{(1,2)} \cdot \vec{\mathrm{I}}_{2\times2}^{-1} \cdot \vec{Q}_{2\times2}^{(2,1)}\right]^{-1} \cdot \vec{Q}_{2\times2}^{(1,2)} \cdot \vec{\mathrm{I}}_{2\times2}^{-1} \\ &= -\vec{A}_{2\times2} \cdot \vec{Q}_{2\times2}^{(1,2)} \\ \vec{D}_{2\times2} &= \left[\vec{\mathrm{I}}_{2\times2} - \vec{Q}_{2\times2}^{(2,1)} \cdot \vec{\mathrm{I}}_{2\times2}^{-1} \cdot \vec{Q}_{2\times2}^{(1,2)}\right]^{-1} \\ \vec{C}_{2\times2} &= -\left[\vec{\mathrm{I}}_{2\times2} - \vec{Q}_{2\times2}^{(2,1)} \cdot \vec{\mathrm{I}}_{2\times2}^{-1} \cdot \vec{Q}_{2\times2}^{(1,2)}\right]^{-1} \cdot \vec{Q}_{2\times2}^{(2,1)} \cdot \vec{\mathrm{I}}_{2\times2}^{-1} \\ &= -\vec{D}_{2\times2} \cdot \vec{Q}_{2\times2}^{(2,1)} \ . \end{aligned} \tag{31}$$

For two interacting dipoles, (28) becomes

$$\begin{aligned} \det\begin{bmatrix} \vec{\mathrm{I}}_{2\times2} & \vec{Q}_{2\times2}^{(1,2)} \\ \vec{Q}_{2\times2}^{(2,1)} & \vec{\mathrm{I}}_{2\times2} \end{bmatrix} &= \det\left[\vec{\mathrm{I}}_{2\times2}\right] \det\left[\vec{\mathrm{I}}_{2\times2} - \vec{Q}_{2\times2}^{(2,1)} \cdot \vec{\mathrm{I}}_{2\times2}^{-1} \cdot \vec{Q}_{2\times2}^{(1,2)}\right] \\ &= \det\left[\vec{\mathrm{I}}_{2\times2} - \vec{Q}_{2\times2}^{(2,1)} \cdot \vec{Q}_{2\times2}^{(1,2)}\right] = 0 \end{aligned} \tag{32}$$

IV. Characteristic equation for thin wires

At this point it is instructive to examine a special case of (32). Consider two non-identical objects with $\vec{M}^{(1)} = \vec{M}^{(2)} = \vec{0}$. In this case the two non-trivial block-dyadics are

$$\ddot{Q}_{2\times 2}^{(\alpha,\beta)} = \begin{bmatrix} -\epsilon_0 \ddot{P}_0^{(\alpha)} \cdot \ddot{F}_{e,e}^{(\alpha,\beta)} & \ddot{0} \\ \ddot{0} & \ddot{0} \end{bmatrix} \tag{33}$$

leading to

$$\det\left[\ddot{1} - \epsilon_0^2 \ddot{P}_0^{(2)} \cdot \ddot{F}_{e,e}^{(2,1)} \cdot \ddot{P}_0^{(1)} \cdot \ddot{F}_{e,e}^{(1,2)}\right] = 0 \ . \tag{34}$$

As an example, consider thin, perfectly conducting wires oriented along the α-direction, for which $\ddot{P}_0 = P_0 \vec{1}_\alpha \vec{1}_\alpha$ and the magnetic polarizability dyadic is negligible. A prolate spheroid model of a wire, with semi-major axis L/2 and semi-minor axis a, results in [14]

$$P_0 = \frac{4}{3}\pi\left(\frac{L}{2}\right)^3\left[1-\left(\frac{2a}{L}\right)\right]\left\{\frac{1}{2}\left[1-\left(\frac{2a}{L}\right)^2\right]^{-1/2}\ln\left[\frac{1+\left[1-\left(\frac{2a}{L}\right)^2\right]^{1/2}}{1-\left[1-\left(\frac{2a}{L}\right)^2\right]^{1/2}}\right]-1\right\}^{-1} \tag{35}$$

$$= \frac{4}{3}\pi\left(\frac{L}{2}\right)^3\left[\ln\left(\frac{L}{a}\right)-1\right]^{-1} \qquad as \ \ \frac{a}{L}\to 0 \ .$$

Now, consider three different orientations of the wires. For simplicity, in each case the wires will be located at $\vec{r}_{\frac{1}{2}} = x_0\vec{1}_x + y_0\vec{1}_y \pm \frac{L}{2}\vec{1}_z$, such that $\ddot{F}_{e,e}^{(2,1)} = \ddot{F}_{e,e}^{(1,2)}$.

Case a. parallel wires:

Consider the wires to be oriented parallel to the x-axis of Fig. 1., such that $\ddot{P}_0^{(\alpha)} = \vec{1}_x\vec{1}_x P_0^{(\alpha)}$ with $P_0^{(\alpha)}$ defined by (35). The governing equation (34) becomes

$$\det\left[\ddot{1} - \epsilon_0^2 \ddot{P}_0^{(2)} \cdot \ddot{F}_{e,e}^{(2,1)} \cdot \ddot{P}_0^{(1)} \cdot \ddot{F}_{e,e}^{(1,2)}\right]$$

$$= 1 - \epsilon_0^2 P_0^{(2)} P_0^{(1)}\left[\left(\frac{e^{-\gamma r}}{4\pi}\right)\left(\frac{1}{r^3\epsilon_0} + \frac{Z_0 s}{r^2} + \frac{\mu_0 s^2}{r}\right)\right]^2 = 0 \ . \tag{36}$$

Making the substitution $\Gamma = \gamma r$, yields

$$e^{-\Gamma}(1+\Gamma+\Gamma^2) = \pm\frac{r^3 4\pi}{\sqrt{P_0^{(2)} P_0^{(1)}}} \tag{37}$$

which is the characteristic equation for the natural system frequencies of two non-identical, parallel wires in the large-separation limit. The solution of (37) for the special case of two identical wires will be considered in Sec. VII and in the appendix. If we further assume the same length-to-radius ratio for both

wires, $L^{(1)}/a^{(1)} = L^{(2)}/a^{(2)} = L_a$, then $P_0^{(1,2)} = K[L^{(1,2)}]^3$ with $K = \frac{\pi}{6}[\ln(L_a) - 1]^{-1}$, (37) can be written more directly in terms of the three parameters $r, L^{(1)}, L^{(2)}$ as

$$e^{-\Gamma}(1+\Gamma+\Gamma^2) = \pm\left(\frac{r}{L^{(2)}}\right)^{\frac{3}{2}}\left(\frac{r}{L^{(1)}}\right)^{\frac{3}{2}}\frac{4\pi}{k}\,. \tag{38}$$

Case b. collinear wires:

Consider two collinear wires aligned parallel to the z-axis of Fig. 1, such that $\vec{\vec{P}}_0^{(\alpha)} = \vec{1}_z\vec{1}_z P_0^{(\alpha)}$ with $P_0^{(\alpha)}$ defined by (35). The governing characteristic equation (34) becomes

$$\begin{aligned}&\det\left[\vec{\vec{1}} - \epsilon_0^2\,\vec{\vec{P}}_0^{(2)}\cdot\vec{\vec{F}}_{e,e}^{(2,1)}\cdot\vec{\vec{P}}_0^{(1)}\cdot\vec{\vec{F}}_{e,e}^{(1,2)}\right]\\ &= 1 - \epsilon_0^2\,P_0^{(2)}\,P_0^{(1)}\left[\left(\frac{e^{-\gamma r}}{2\pi}\right)\left(\frac{1}{r^3\epsilon_0} + \frac{Z_0 S}{r^2}\right)\right]^2 = 0\end{aligned} \tag{39}$$

resulting in

$$e^{-\Gamma}(1+\Gamma) = \pm\,\frac{r^3 2\pi}{\sqrt{P_0^{(2)}\,P_0^{(1)}}} \tag{40}$$

which is the characteristic equation for the natural system frequencies of two non-identical, collinear wires in the large-separation limit. The solution of (40) for the special case of two identical wires will be considered in the appendix. For $L^{(1)}/a^{(1)} = L^{(2)}/a^{(2)} = L_a$, such that $P_0^{(1,2)} = K[L^{(1,2)}]^3$ with k as defined previously, (40) can be written as

$$e^{-\Gamma}(1+\Gamma) = \pm\left(\frac{r}{L^{(2)}}\right)^{\frac{3}{2}}\left(\frac{r}{L^{(1)}}\right)^{\frac{3}{2}}\frac{2\pi}{k}\,. \tag{41}$$

Case c. perpendicularly-oriented wires:

To analyze two wires oriented perpendicularly to each other, one may take, for instance, $\vec{\vec{P}}_0^{(1)} = \vec{1}_x\vec{1}_x P_0^{(1)}$ and $\vec{\vec{P}}_0^{(2)} = \vec{1}_z\vec{1}_z P_0^{(2)}$. The characteristic equation (34) becomes

$$\det\left[\vec{\vec{1}} - \epsilon_0^2\,\vec{\vec{P}}_0^{(2)}\cdot\vec{\vec{F}}_{e,e}^{(2,1)}\cdot\vec{\vec{P}}_0^{(1)}\cdot\vec{\vec{F}}_{e,e}^{(1,2)}\right] = \det[\vec{\vec{1}} - \vec{\vec{0}}] = 1 \tag{42}$$

so that no frequency exists to yield a singular matrix.

V. Scattering from a dipole in the presence of a mirror object

In this section we will specialize the preceding formulation to the case of two interacting dipoles

which are mirror images of each other, as shown in Fig. 2. For simplicity, each dipole is located at x=y=0, so that dipole 1 is located at $\vec{r}_1 = \vec{1}_z\, r/2$, and dipole two is located at $\vec{r}_2 = -\vec{1}_z\, r/2 = \vec{\vec{R}}_z \cdot \vec{r}_1$, such that $\vec{1}_{R_{1,2}} = \vec{1}_z = -\vec{1}_{R_{1,1}}$, where [15]

$$\vec{\vec{R}}_z \equiv \begin{bmatrix} 1 & 0 & 0 \\ 0 & 1 & 0 \\ 0 & 0 & -1 \end{bmatrix} = \vec{\vec{R}}_z^{-1} . \tag{43}$$

The incident fields can be decomposed into symmetric and antisymmetric parts as [14]

$$\begin{aligned}
\vec{E}^{(inc)}(\vec{r}_1, s) &= \frac{1}{2}\left[\vec{E}^{(inc)}(\vec{r}_1, s) \pm \vec{\vec{R}}_z \cdot \vec{E}^{(inc)}(\vec{r}_2, s)\right] \\
\vec{E}^{(inc)}(\vec{r}_2, s) &= \frac{1}{2}\left[\vec{E}^{(inc)}(\vec{r}_2, s) \pm \vec{\vec{R}}_z \cdot \vec{E}^{(inc)}(\vec{r}_1, s)\right] \\
\vec{H}^{(inc)}(\vec{r}_1, s) &= \frac{1}{2}\left[\vec{H}^{(inc)}(\vec{r}_1, s) \mp \vec{\vec{R}}_z \cdot \vec{H}^{(inc)}(\vec{r}_2, s)\right] \\
\vec{H}^{(inc)}(\vec{r}_2, s) &= \frac{1}{2}\left[\vec{H}^{(inc)}(\vec{r}_2, s) \mp \vec{\vec{R}}_z \cdot \vec{H}^{(inc)}(\vec{r}_1, s)\right] .
\end{aligned} \tag{44}$$

From the above it is easily seen that

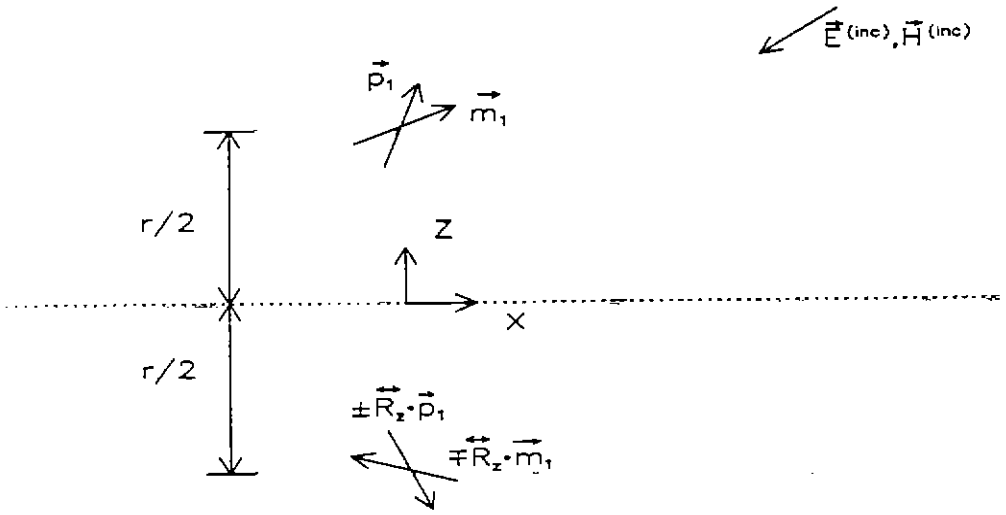

Fig. 2. Two mirror-symmetric dipoles, upper sign depicted.

$$
\begin{aligned}
\vec{E}^{(inc)}(\vec{r}_1, s) &= \pm \ddot{R}_z \cdot \vec{E}^{(inc)}(\vec{r}_2, s) \\
\vec{E}^{(inc)}(\vec{r}_2, s) &= \pm \ddot{R}_z \cdot \vec{E}^{(inc)}(\vec{r}_1, s) \\
\vec{H}^{(inc)}(\vec{r}_1, s) &= \mp \ddot{R}_z \cdot \vec{H}^{(inc)}(\vec{r}_2, s) \\
\vec{H}^{(inc)}(\vec{r}_2, s) &= \mp \ddot{R}_z \cdot \vec{H}^{(inc)}(\vec{r}_1, s) \ .
\end{aligned}
\tag{45}
$$

With the relations

$$
\begin{aligned}
\ddot{F}_{e,e} &\equiv \ddot{F}_{e,e}(\vec{r}_\alpha | \vec{r}_\beta, s) = \ddot{R}_z \cdot \ddot{F}_{e,e}(\vec{r}_\beta | \vec{r}_\alpha, s) \cdot \ddot{R}_z \\
\ddot{P}_0^{(\alpha)} &= \ddot{R}_z \cdot \ddot{P}_0^{(\beta)} \cdot \ddot{R}_z \\
\ddot{M}_0^{(\alpha)} &= \ddot{R}_z \cdot \ddot{M}_0^{(\beta)} \cdot \ddot{R}_z \\
\vec{p}^{(\alpha)} &= \pm \ddot{R}_z \cdot \vec{p}^{(\beta)} = \pm \vec{p}^{(\beta)} \cdot \ddot{R}_z \\
\vec{m}^{(\alpha)} &= \mp \ddot{R}_z \cdot \vec{m}^{(\beta)} = \mp \vec{m}^{(\beta)} \cdot \ddot{R}_z \qquad \alpha \neq \beta
\end{aligned}
\tag{46}
$$

the scattered fields are related by

$$
\begin{aligned}
\vec{E}^{(\alpha,\beta)}(\vec{r}_\alpha, s) &= \pm \ddot{R}_z \cdot \vec{E}^{(\beta,\alpha)}(\vec{r}_\beta, s) \\
\vec{H}^{(\alpha,\beta)}(\vec{r}_\alpha, s) &= \mp \ddot{R}_z \cdot \vec{H}^{(\beta,\alpha)}(\vec{r}_\beta, s) \ .
\end{aligned}
\tag{47}
$$

With (45)-(47), (23) becomes

$$
\begin{aligned}
&\vec{p}^{(1)}(s) \mp \epsilon_0 \ddot{P}_0^{(1)} \cdot \left[\ddot{F}_{e,e} \cdot \ddot{R}_z \cdot \vec{p}^{(1)} - F_{e,m} (\vec{1}_z \times \ddot{R}_z) \cdot \vec{m}^{(1)} \right] = \epsilon_0 \ddot{P}_0^{(1)} \cdot \vec{E}^{(inc)}(\vec{r}_1, s) \\
&\vec{m}^{(1)}(s) \pm \ddot{M}_0^{(1)} \cdot \left[\frac{1}{\mu_0} F_{e,m} (\vec{1}_z \times \ddot{R}_z) \cdot \vec{p}^{(1)} + \epsilon_0 \ddot{F}_{e,e} \cdot \ddot{R}_z \cdot \vec{m}^{(1)} \right] = \ddot{M}_0^{(1)} \cdot \vec{H}^{(inc)}(\vec{r}_1, s)
\end{aligned}
\tag{48}
$$

which can be written in matrix form as

$$
\begin{bmatrix}
\ddot{1} \mp \epsilon_0 \ddot{P}_0^{(1)} \cdot \ddot{F}_{e,e} \cdot \ddot{R}_z & \pm \epsilon_0 F_{e,m} \ddot{P}_0^{(1)} \cdot (\vec{1} \times \ddot{R}_z) \\
\pm \frac{1}{\mu_0} F_{e,m} \ddot{M}_0^{(1)} \cdot (\vec{1}_z \times \ddot{R}_z) & \ddot{1} \pm \epsilon_0 \ddot{M}_0^{(1)} \cdot \ddot{F}_{e,e} \cdot \ddot{R}_z
\end{bmatrix}
\cdot
\begin{bmatrix}
\vec{p}^{(1)}(s) \\ \vec{m}^{(1)}(s)
\end{bmatrix}
=
\begin{bmatrix}
\epsilon_0 \ddot{P}_0^{(1)} \cdot \vec{E}^{(inc)} \\ \ddot{M}_0^{(1)} \cdot \vec{H}^{(inc)}
\end{bmatrix} .
\tag{49}
$$

Equation (49) is naturally decomposed into block dyadic form as

$$
\begin{bmatrix}
\ddot{Q}_{pp}(s) & \ddot{Q}_{pm}(s) \\
\ddot{Q}_{mp}(s) & \ddot{Q}_{mm}(s)
\end{bmatrix}
\cdot
\begin{bmatrix}
\vec{p}^{(1)}(s) \\ \vec{m}^{(1)}(s)
\end{bmatrix}
=
\begin{bmatrix}
\epsilon_0 \ddot{P}_0^{(1)} \cdot \vec{E}^{(inc)}(s) \\ \ddot{M}_0^{(1)} \cdot \vec{H}^{(inc)}(s)
\end{bmatrix}
\tag{50}
$$

where

$$
\begin{aligned}
\ddot{Q}_{pp}(s) &\equiv \ddot{1} \mp \epsilon_0 \ddot{P}_0^{(1)} \cdot \ddot{F}_{e,e} \cdot \ddot{R}_z \\
\ddot{Q}_{pm}(s) &\equiv \pm \epsilon_0 F_{e,m} \ddot{P}_0^{(1)} \cdot (\vec{1} \times \ddot{R}_z) \\
\ddot{Q}_{mp}(s) &\equiv \pm \frac{1}{\mu_0} F_{e,m} \ddot{M}_0^{(1)} \cdot (\vec{1}_z \times \ddot{R}_z) \\
\ddot{Q}_{mm}(s) &\equiv \ddot{1} \pm \epsilon_0 \ddot{M}_0^{(1)} \cdot \ddot{F}_{e,e} \cdot \ddot{R}_z
\end{aligned}
\tag{51}
$$

such that each block is a single dyadic expression rather than a matrix of dyadics as in (24). Providing that the left-hand dyadic matrix is non-singular, (50) can be inverted in the same manner as (29) to yield

$$
\begin{bmatrix} \vec{p}^{(1)}(s) \\ \vec{m}^{(1)}(s) \end{bmatrix} = \begin{bmatrix} \ddot{Q}_{pp}(s) & \ddot{Q}_{pm}(s) \\ \ddot{Q}_{mp}(s) & \ddot{Q}_{mm}(s) \end{bmatrix}^{-1} \cdot \begin{bmatrix} \epsilon_0 \ddot{P}_0^{(1)} \cdot \vec{E}^{(inc)}(s) \\ \ddot{M}_0^{(1)} \cdot \vec{H}^{(inc)}(s) \end{bmatrix} \tag{52}
$$

where

$$
\begin{bmatrix} \ddot{Q}_{pp} & \ddot{Q}_{pm} \\ \ddot{Q}_{mp} & \ddot{Q}_{mm} \end{bmatrix}^{-1} = \begin{bmatrix} \ddot{A} & \ddot{B} \\ \ddot{C} & \ddot{D} \end{bmatrix} \tag{53}
$$

with

$$
\begin{aligned}
\ddot{A} &= \left[\ddot{Q}_{pp} - \ddot{Q}_{pm} \cdot \ddot{Q}_{mm}^{-1} \cdot \ddot{Q}_{mp}\right]^{-1} \\
\ddot{B} &= -\left[\ddot{Q}_{pp} - \ddot{Q}_{pm} \cdot \ddot{Q}_{mm}^{-1} \cdot \ddot{Q}_{mp}\right]^{-1} \cdot \ddot{Q}_{pm} \cdot \ddot{Q}_{mm}^{-1} \\
&= -\ddot{A} \cdot \ddot{Q}_{pm} \cdot \ddot{Q}_{mm}^{-1} \\
\ddot{D} &= \left[\ddot{Q}_{mm} - \ddot{Q}_{mp} \cdot \ddot{Q}_{pp}^{-1} \cdot \ddot{Q}_{pm}\right]^{-1} \\
\ddot{C} &= -\left[\ddot{Q}_{mm} - \ddot{Q}_{mp} \cdot \ddot{Q}_{pp}^{-1} \cdot \ddot{Q}_{pm}\right]^{-1} \cdot \ddot{Q}_{mp} \cdot \ddot{Q}_{pp}^{-1} \\
&= -\ddot{D} \cdot \ddot{Q}_{mp} \cdot \ddot{Q}_{pp}^{-1} .
\end{aligned}
\tag{54}
$$

Equation (52) provides a formal solution to the mirror-symmetric scattering problem for configurations and frequencies such that the dipole moment approximation is valid. As in Sec. III, we are primarily interested in determining the natural frequencies such that the left-hand dyadic matrix is singular, leading to

$$
\det \begin{bmatrix} \ddot{Q}_{pp} & \ddot{Q}_{pm} \\ \ddot{Q}_{mp} & \ddot{Q}_{mm} \end{bmatrix} = \det\left[\ddot{Q}_{pp}\right] \det\left[\ddot{Q}_{mm} - \ddot{Q}_{mp} \cdot \ddot{Q}_{pp}^{-1} \cdot \ddot{Q}_{pm}\right] = 0 \tag{55}
$$

which forms the fundamental characteristic equation for natural system frequencies of two interacting mirror-symmetric objects in the large separation, low frequency regime. In the following section, mirror-

symmetric configurations of wires and loops will be considered. It should be noted in all of the results to follow, the upper and lower signs correspond to the symmetric and anti-symmetric modes, respectively.

VI. Characteristic equation for mirror-symmetric wires and loops

Consider a thin, perfectly conducting wire with $\vec{\vec{M}}^{(1)} = \vec{\vec{0}}$. Equation (55) reduces to

$$\det[\vec{\vec{Q}}_{pp}] = \det\left[\vec{\vec{1}} \mp \epsilon_0 \vec{\vec{P}}_0^{(1)} \cdot \vec{\vec{F}}_{e,e} \cdot \vec{\vec{R}}_z\right] = 0 \tag{56}$$

which can be written in matrix form as

$$\det\begin{bmatrix} 1 \pm \epsilon_0 \frac{e^{-\gamma r}}{4\pi} P_{xx}(a_1 + b_1) & \pm \epsilon_0 P_{xy}(a_1 + b_1) & \pm \epsilon_0 P_{xz} 2a_1 \\ \pm \epsilon_0 P_{yx}(a_1 + b_1) & 1 \pm \epsilon_0 \frac{e^{-\gamma r}}{4\pi} P_{yy}(a_1 + b_1) & \pm \epsilon_0 P_{yz} 2a_1 \\ \pm \epsilon_0 P_{zx}(a_1 + b_1) & \pm \epsilon_0 P_{zy}(a_1 + b_1) & 1 \pm \epsilon_0 \frac{e^{-\gamma r}}{4\pi} P_{zz} 2a_1 \end{bmatrix} = 0 \tag{57}$$

where

$$a_1 = \frac{1}{r^3 \epsilon_0} + \frac{Z_0 s}{r^2}, \quad b_1 = \frac{\mu_0 s^2}{r}. \tag{58}$$

Now consider three different wire orientations.

Case a. parallel wires:

Consider two parallel wires oriented along the x-axis of Fig. 2, such that $\vec{\vec{P}}_0^{(1)} = \vec{1}_x \vec{1}_x P_0$ with P_0 defined by (35). Equation (57) then becomes

$$1 \pm \epsilon_0 \frac{e^{-\gamma r}}{4\pi} P_0 \left(\frac{1}{r^3 \epsilon_0} + \frac{Z_0 s^2}{r^2} + \frac{\mu_0 s^2}{r} \right) = 0. \tag{59}$$

With $\Gamma = \gamma r$ as defined before, we get

$$e^{-\Gamma}(1 + \Gamma + \Gamma^2) = \mp \frac{r^3 4\pi}{P_0} \tag{60}$$

which is the characteristic equation for the natural system frequencies of two identical, parallel wires in the large-separation limit. Although this is merely a special case of (37) with $P_0^{(2)} = P_0^{(1)} = P_0$, it should be noted that the mirror-symmetric formulation leading to (60) is simpler than the general scattering formulation, justifying the usefulness of the separate derivation outlined in this section. The solution of (37) for the special case of two identical wires, i.e., (60), will be considered in Sec. VII and in the appendix.

Case b. collinear wires:

Consider two collinear wires aligned along the z-axis of Fig. 2, such that $\vec{P}_0^{(1)} = \vec{1}_z \vec{1}_z P_0$ with P_0 defined by (35). The governing characteristic equation (57) reduces to

$$1 \pm \epsilon_0 \frac{e^{-\gamma r}}{4\pi} 2P_0 \left(\frac{1}{r^3 \epsilon_0} + \frac{Z_0 s^2}{r^2} \right) = 0 \tag{61}$$

which can be written as

$$e^{-\Gamma}(1+\Gamma) = \mp \frac{r^3 2\pi}{P_0} \tag{62}$$

which is the characteristic equation for the natural system frequencies of two identical, collinear wires in the large-separation limit. Note that (62) is merely a special case of (40) with $P_0^{(2)} = P_0^{(1)} = P_0$, although derived under the simpler mirror-symmetric formulation. The solution of (40) for the special case of two identical wires, i.e., (62), will be considered in the appendix.

Case c. mirror-symmetric wires arbitrary oriented in the x-z plane:

Consider one of the wires to lie in the x-z plane in Fig. 2, at an angle θ measured from the z-axis, with the other wire in mirror-symmetric fashion. The polarizability dyadic for this case is

$$\begin{aligned} \vec{P}_0^{(1)} &= \vec{1}_{z'} \vec{1}_{z'} P_0 \\ &= \left[\vec{1}_z \vec{1}_z \cos^2(\theta) + \vec{1}_z \vec{1}_x \cos(\theta)\sin(\theta) + \vec{1}_x \vec{1}_z \cos(\theta)\sin(\theta) + \vec{1}_x \vec{1}_x \sin^2(\theta) \right] P_0 \\ &= \vec{1}_z \vec{1}_z P_{zz} + \vec{1}_z \vec{1}_x P_{zx} + \vec{1}_x \vec{1}_z P_{xz} + \vec{1}_x \vec{1}_x P_{xx} \end{aligned} \tag{63}$$

with P_0 defined by (35). The relevant characteristic equation (57) then becomes

$$\det \begin{bmatrix} 1 \pm \epsilon_0 \frac{e^{-\gamma r}}{4\pi} P_{xx}(a_1 + b_1) & 0 & \pm \epsilon_0 \frac{e^{-\gamma r}}{4\pi} P_{xz} 2a_1 \\ 0 & 1 & 0 \\ \pm \epsilon_0 \frac{e^{-\gamma r}}{4\pi} P_{zx}(a_1 + b_1) & 0 & 1 \pm \epsilon_0 \frac{e^{-\gamma r}}{4\pi} P_{zz} 2a_1 \end{bmatrix} = 0 \tag{64}$$

leading to

$$e^{-\Gamma}\{\sin^2(\theta)\,(1+\Gamma+\Gamma^2) + \cos^2(\theta)\,2(1+\Gamma)\} = \mp \frac{r^3 4\pi}{P_0}\,. \tag{65}$$

Note that (65) reduces to (62) for $\theta = 0$, and to (60) for $\theta = \pi/2$, as expected.

As another example, consider two parallel thin-wire loops with axes aligned along the z-axis of Fig. 2, separated by a distance r, each having loop radius b and wire radius a. The polarizability dyadics are

$$\begin{aligned} \vec{P}^{(1)} &= \vec{1}_x \vec{1}_x P_{xx} + \vec{1}_y \vec{1}_y P_{yy} \\ \vec{M}^{(1)} &= \vec{1}_z \vec{1}_z M_{zz} \end{aligned} \tag{66}$$

which from (55) leads to

$$\det \begin{bmatrix} 1 \pm \epsilon_0 \frac{e^{-\gamma r}}{4\pi} P_{xx}(a_1 + b_1) & 0 & 0 & 0 \\ 0 & 1 \pm \epsilon_0 \frac{e^{-\gamma r}}{4\pi} P_{yy}(a_1 + b_1) & 0 & \pm \epsilon_0 \frac{e^{-\gamma r}}{4\pi} F_{e,m} 2 M_{zz} \\ 0 & 0 & 1 & 0 \\ 0 & 0 & 0 & 1 \\ 0 & 0 & 0 & 0 \\ 0 & 0 & 0 & 0 \end{bmatrix}$$

$$\begin{bmatrix} \pm \epsilon_0 \frac{e^{-\gamma r}}{4\pi} F_{e,m} 2 M_{zz} & 0 \\ 0 & 0 \\ 0 & 0 \\ 0 & 0 \\ 1 & 0 \\ 0 & 1 \mp \epsilon_0 \frac{e^{-\gamma r}}{4\pi} M_{zz} 2 a_1 \end{bmatrix} = 0 . \tag{67}$$

Since the determinant will vanish if any diagonal entry is zero, (67) leads to

$$\begin{aligned} e^{-\Gamma}(1 + \Gamma + \Gamma^2) &= \pm \frac{r^3 4\pi}{P_{xx}} \\ e^{-\Gamma}(1 + \Gamma + \Gamma^2) &= \pm \frac{r^3 4\pi}{P_{yy}} \end{aligned} \tag{68}$$

which are essentially the same as (60) with a sign change, and

$$e^{-\Gamma}(1 + \Gamma) = \pm \frac{r^3 2\pi}{M_{zz}} \tag{69}$$

which is the similar to (62) with a sign change and P_0 replaced with M_{zz}. The polarizability terms in (66) are related by $P_{xx} = P_{yy} = -2M_{zz}$ [16], with

$$M_{zz} = -\pi^2 b^3 \left[\ln\left(\frac{8b}{a}\right) - 2 \right]^{-1}. \qquad (70)$$

VII. Numerical results

In order to demonstrate the accuracy of the presented formulation, the example of two identical, thin, perfectly conducting parallel wires separated by a distance r=d is considered, as depicted in the insert of Fig. 3. The wires are in a mirror-symmetric configuration, which admits pure symmetric and antisymmetric modes. In all results to follow, both wires have L/a=200, and the natural frequencies in the upper-half s-plane will be considered. For one such wire when isolated, the dominant resonance is at $\frac{s_{1,1}^0 L}{c\pi} = -0.0865 + j0.9386$, computed from a rigorous electric-field integral equation (IE) using a pulse basis and point matching [17]. Other resonances are available in the literature, e.g. [1].

For the coupled wire configuration described above, the asymptotic formulation (60) becomes

$$e^{-\Gamma}(1+\Gamma+\Gamma^2) = \mp 103.1596 \left(\frac{d}{L}\right)^3 \qquad (71)$$

for L/a=200. The migration of the lowest-order anti-symmetric and symmetric mode as a function of spacing d/L is shown in Fig.'s, 3 and 4, respectively. The solid line is the solution from the integral equation [16], the dashed line is from the perturbation solution formulated in [6], while the dotted line is the solution of (71). The solid box is the location of the isolated body resonance, $\frac{s_{1,1}^0 L}{c\pi}$. It can be seen that the spiraling behavior is essentially well described by the perturbation solution for intermediate spacings, and the asymptotic solution agrees very well for larger spacings, as expected.

Fig.'s 5-8 show the radian frequency and damping coefficient for the lowest-order anti-symmetric and symmetric mode versus spacing d/L. For the modes considered in these figures, the asymptotic formulation (71) agrees very well with the exact solution for d/L > 10. For all of the IE solutions presented, 20 pulses were used to generate the natural frequencies.

For the results in Fig.'s 3-8, (71) was solved numerically using initial guesses generated from the approximate solution (A.11) obtained in the appendix, which becomes

$$\Gamma_m^{\binom{sy}{as}} = \frac{s_m^{\binom{sy}{as}}}{c} d = \ln\left[0.02392 m^2 \left(\frac{L}{d}\right)^3 \right] + j\frac{m\pi}{2} \qquad m = \begin{pmatrix} 4, 8, 12, \ldots \\ 2, 6, 10, \ldots \end{pmatrix} \qquad (72)$$

for L/a=200. A comparison of the approximate solution (72) to the numerical solution of (71), and to the IE solution is provided in Tables 1-2 for d/L=10, and Tables 3-4 for d/L=100. The numerical solution of (71) was generated with a secant-method root search. It can be seen that the agreement between the numerical solution of (71) and the IE solution is very good, and is nearly perfect for the real radian frequency for the larger d/L value. This indicates the accuracy of the asymptotic formulation.

Concerning the approximate solution (72), it can be seen that the results are very good for higher-order modes (larger m values), although not as accurate for lower-order modes. For the real part, this is expected due to the assumption $\frac{m\pi}{2} \gg |\Gamma_r|$ used in obtaining Γ_r in the appendix. For higher-order modes, m approaches an integer value, thereby making the solution accurate for Γ_i as well. The last column of each table shows the actual value of m obtained from the IE solution. With these non-integer values, (72) would yield natural frequencies closer to the numerical solution of (71).

14	-5.36+j21.99	-5.28+j22.41	-4.28+j22.64	14.41

Table 2. Γ_m, Symmetric modes (d/L=10)

m	Approximate soln. (72)	Numerical soln. of (71)	IE soln.	$\frac{Im\{\Gamma_m^{IE}\}}{\pi/2}$
4	-7.87+j6.28	-6.93+j7.68	-6.79+j7.78	4.95
8	-6.48+j12.57	-6.19+j13.37	-5.86+j13.53	8.61
12	-5.67+j18.85	-5.55+j19.35	-4.87+j19.57	12.46
16	-5.10+j25.13	-5.04+j25.49	-3.50+j25.67	16.34

Table 3. Γ_m, Antisymmetric modes (d/L=100)

m	Approximate soln. (72)	Numerical soln. of (71)	IE soln.	$\frac{Im\{\Gamma_m^{IE}\}}{\pi/2}$
2	-16.16+j3.14	-13.20+j5.47	-13.08+j5.47	3.48
6	-13.97+j9.43	-12.83+j11.10	-12.71+j11.10	7.07
10	-12.94+j15.71	-12.39+j16.93	-12.27+j16.92	10.77
14	-12.27+j21.99	-11.97+j22.92	-11.83+j22.92	14.59

Table 4. Γ_m, Symmetric modes (d/L=100)

m	Approximate soln. (72)	Numerical soln. of (71)	IE soln.	$\frac{Im\{\Gamma_m^{IE}\}}{\pi/2}$
4	-14.78+j6.28	-13.03+j8.26	-12.91+j8.26	5.26
8	-13.39+j12.57	-12.62+j13.99	-12.49+j13.99	8.91
12	-12.56+j18.85	-12.17+j19.91	-12.05+j19.91	12.68
16	-12.00+j25.13	-11.77+j25.95	-11.63+j25.95	16.52

The use of integer m-values in (72) provides a method for classifying the system modes based on their behavior for large separations. In Fig. 9, a portion of the trajectories of the modes m=2 through m=38 are shown. Each curve begins at d/L=100, with d/L decreasing in the direction shown by the arrow. At these d/L values, the asymptotic formulation and the IE solution yield virtually identical results. It can be seen that for any given large separation, these modes form a layer near to the $j\omega$ axis. As d/L decreases, these modes have the following behavior, as obtained from the IE solution. Modes m=2,4,10-24,30-38 move upwards and to the left in the s-plane in such a manner as to form a layer for any given small separation (d/L=1, say). For small separations, this layer is just to the left of the isolated wire first layer for sufficiently small spacing, forming a "secondary layer" [2]. Modes m=6 (antisymmetric) and m=8 (symmetric) become the lowest-order anti-symmetric and symmetric modes, respectively, for small spacing. These modes spiral about, then terminate near, $s_{1,1}^0$ as d/L→0, as shown in Fig.'s 3 and 4, and in Fig. 11, which is discussed below. More specifically, the symmetric mode terminates near $s_{1,1}^0$, and the antisymmetric mode terminates with the real part tending towards zero. These are the modes which have received the most attention in the literature [5],[6]. In Fig.'s 3 and 4, these modes were called the lowest order anti-symmetric and symmetric modes, which is a valid designation only for small spacing. Thus, mode ordering for coupled wires is spacing dependent.

Modes m=26 (antisymmetric) and m=28 (symmetric) behave in a similar manner to m=6 and m=8, but spiral about, then terminate, near $s_{1,2}^0$ as d/L→0, as shown in Fig. 10, and together with m=6 and m=8 in Fig. 11. As with m=6 (the "lowest-order" anti-symmetric mode for small spacing), the anti-symmetric mode m=26 terminates at Re(s)=0, Im(s)≈Im($s_{1,2}^0$) as d/L→0.

In a similar manner, modes m=44 (symmetric) and m=46 (antisymmetric) spiral about, then terminate near, $s_{1,3}^0$ as d/L→0, as shown in Fig. 12, where again the antisymmetric mode m=46 terminates at Re(s)=0, Im(s)≈Im($s_{1,3}^0$) as d/L→0. Several of the low-valued m-modes are shown in Fig.'s 13 and 14, where a comparison between the IE-solution and the asymptotic formulation is made. It can be seen that as m decreases, the asymptotic formulation begins to agree with the IE solution for smaller d/L values.

The natural mode current distribution of the first four m-values for symmetric modes are shown in Fig.'s 15 and 16 for d/L=10, and in Fig.'s 17-18 for d/L=100, obtained from the IE solution. It can be seen that all of the modes have associated dominant-like current distributions for large separations (which lead to low system frequencies), as would be expected. As d/L→∞, the current becomes nearly real, and identical for each natural mode.

To summarize, the system modes of two parallel-coupled, identical wires, which are represented by the solution of (60) for large separations, seem to be divided into several categories.

One group, represented by m=6,8,26,28,44,46, etc., is such that the modes are located near the origin for large separations, and move into the s-plane as separation decreases. These modes spiral about some first layer pole of the isolated wire, $s_{1,n}^{0}$. This has been clearly shown in the literature for the m=6 and m=8 modes, e.g. [2],[5],[6]. Another group of modes, m=2,4,10-24,30-38, etc., are located near the origin for large wire separation, and also move into the s-plane as separation decreases. Each mode maintains its position in a "layer," with the layer moving upwards and to the left as separation decreases. These modes don't spiral about, but may interact with, an isolated wire natural frequency, and form what was called a "secondary layer" in [2]. Both sets of modes are well described by the asymptotic formulation presented here for large d/L values. Other modes also exist, which begin near the origin for large wire separations, but are more heavily damped than the modes described by (72). These modes move off into the s-plane as separation diminishes, and remain more heavily damped, i.e., reside to the left of, both types of modes described by (72). These modes are generally of less interest due to their heavy damping.

VI. Conclusion

In this note we have examined the natural system frequencies of coupled bodies in the limit of large separation between all bodies. The general N-body problem is treated in the limit by replacing the bodies with equivalent dipole moments and solving the relevant scattering problem. Singular solutions of the scattering formulation lead to a transcendental equation which may be solved to obtain the natural system frequencies of the coupled bodies. It has been found for two coupled wires that the real radian system frequency approaches the origin as $1/r$, independent of the relative orientation and type of the two bodies, and that the damping coefficient approaches the origin approximately logarithmically, as a function of the body orientation and type. The asymptotic formulation is applied to the example of two parallel-coupled wires, and a comparison between the asymptotic formulation and an integral equation solution is made, indicating the accuracy of the asymptotic formulation in the appropriate range. For completeness, further results from the IE solution of the two-wire problem are provided for small wire separation, to show the evolution of the modes obtained from the asymptotic formulation beyond its range of validity.

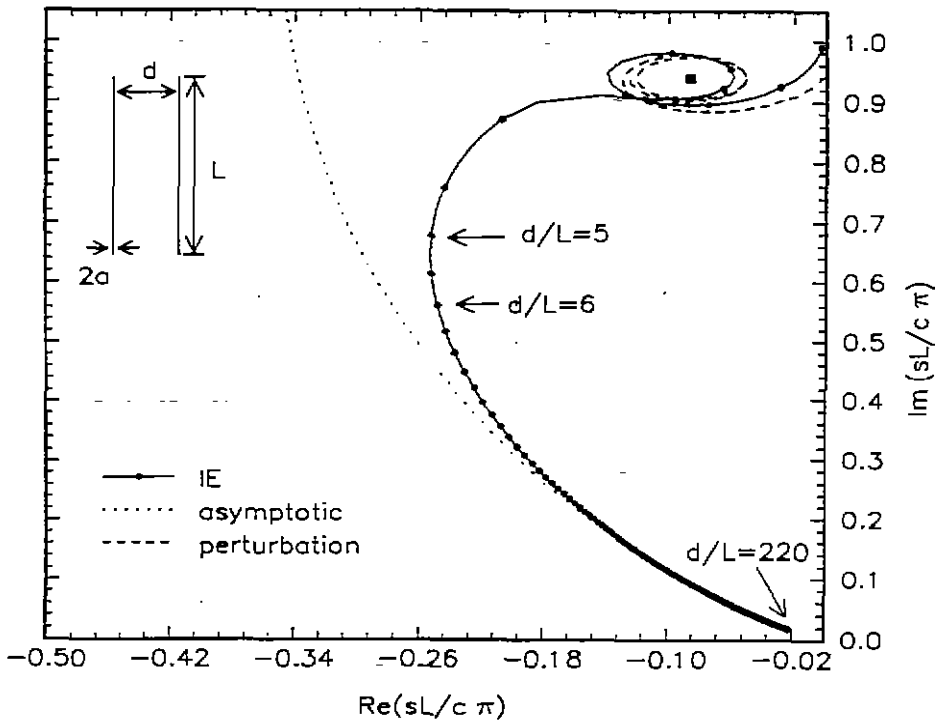

Fig. 3. Trajectory of lowest order anti-symmetric mode of two identical parallel wires parameterized by separation distance, which varies from d/L=220 to d/L=0.01. Solid box is the location of the isolated-wire dominant natural resonance.

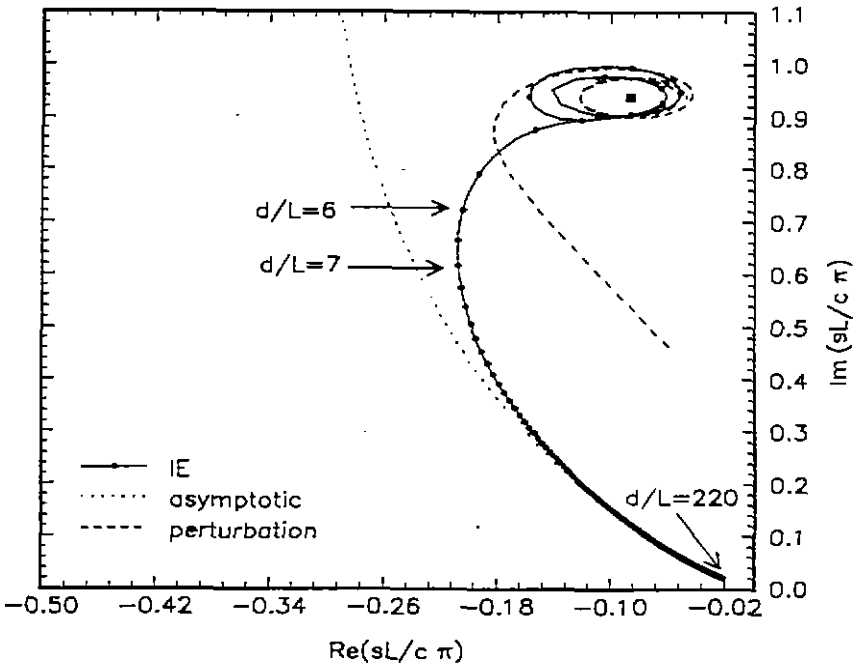

Fig. 4. Trajectory of lowest order symmetric mode of two identical parallel wires parameterized by separation distance, which varies from d/L=220 to d/L=0.01. Solid box is the location of the isolated-wire dominant natural resonance.

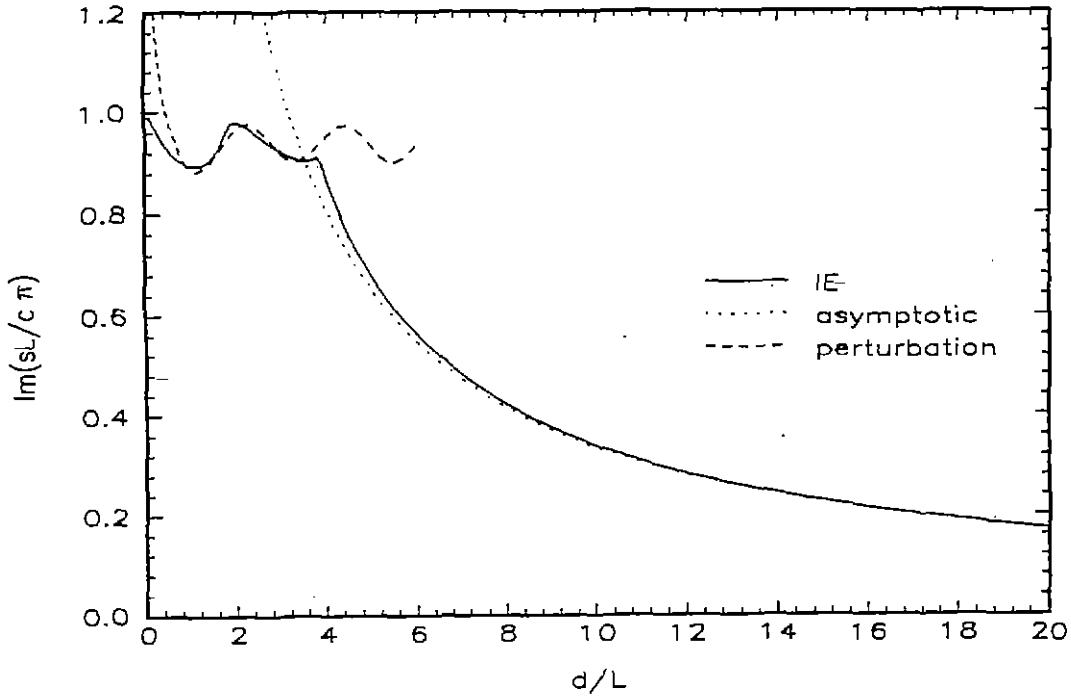

Fig. 5. Radian frequency of lowest order anti-symmetric mode of two identical parallel wires versus separation distance.

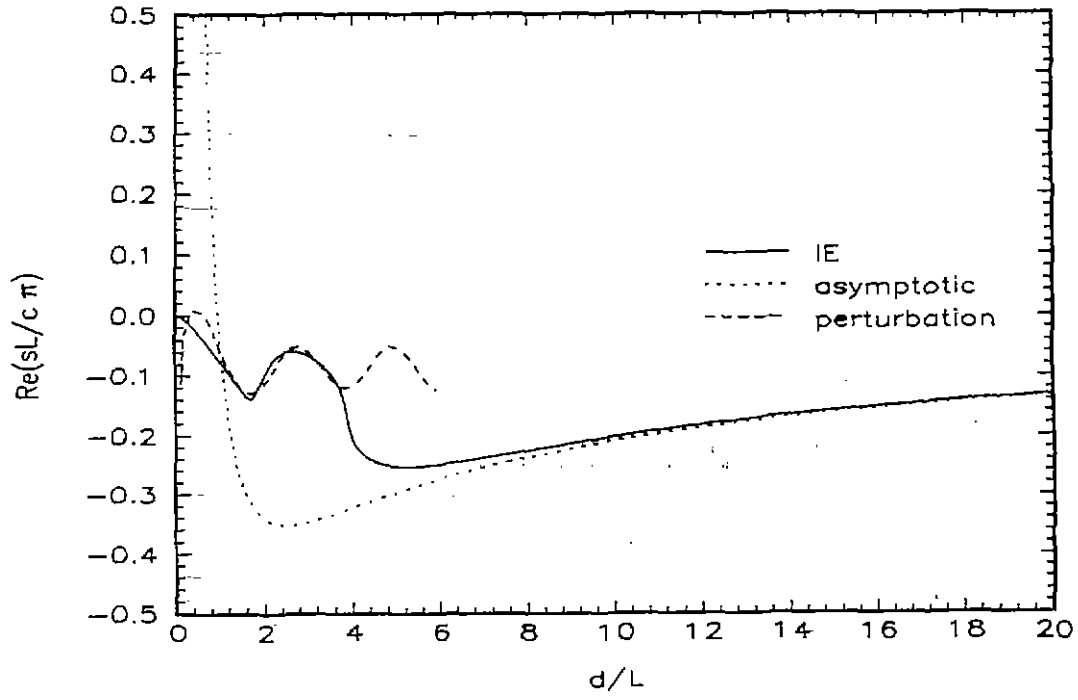

Fig. 6. Damping coefficient of lowest order anti-symmetric mode of two identical parallel wires versus separation distance.

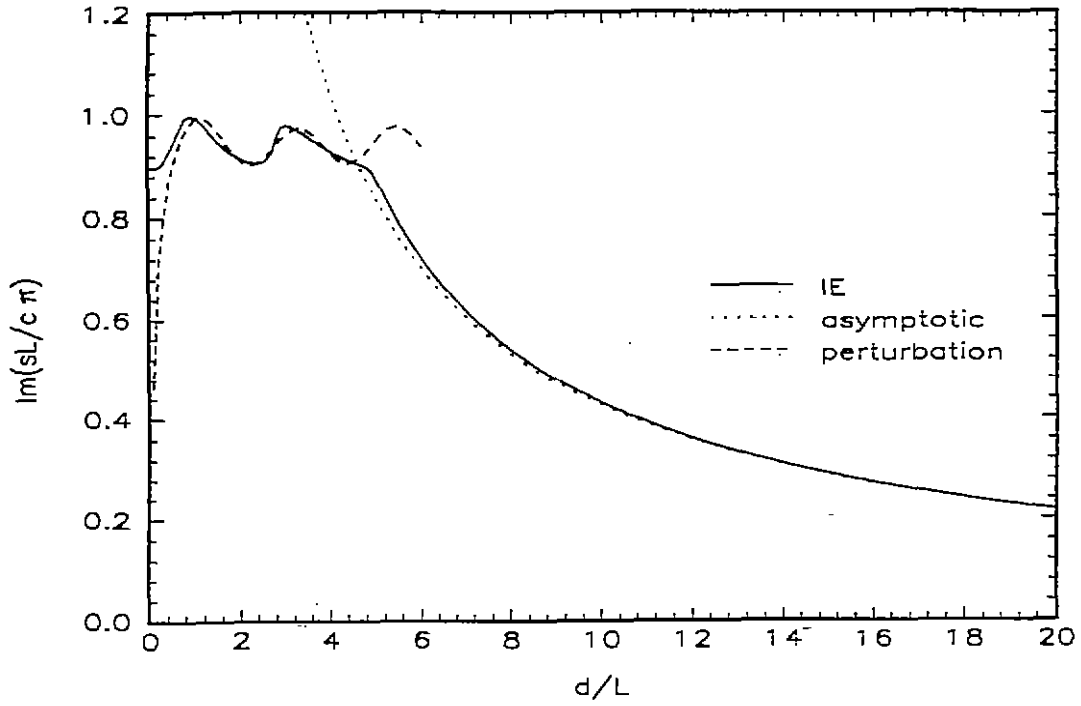

Fig. 7. Radian frequency of lowest order symmetric mode of two identical parallel wires versus separation distance.

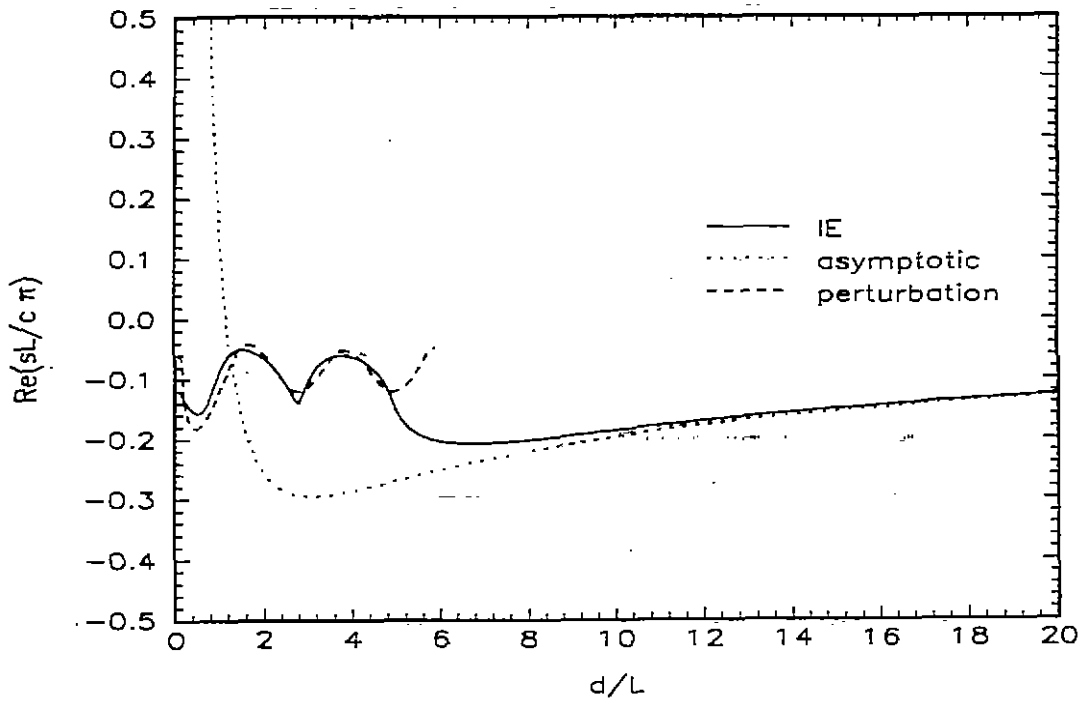

Fig. 8. Damping coefficient of lowest order symmetric mode of two identical parallel wires versus separation distance.

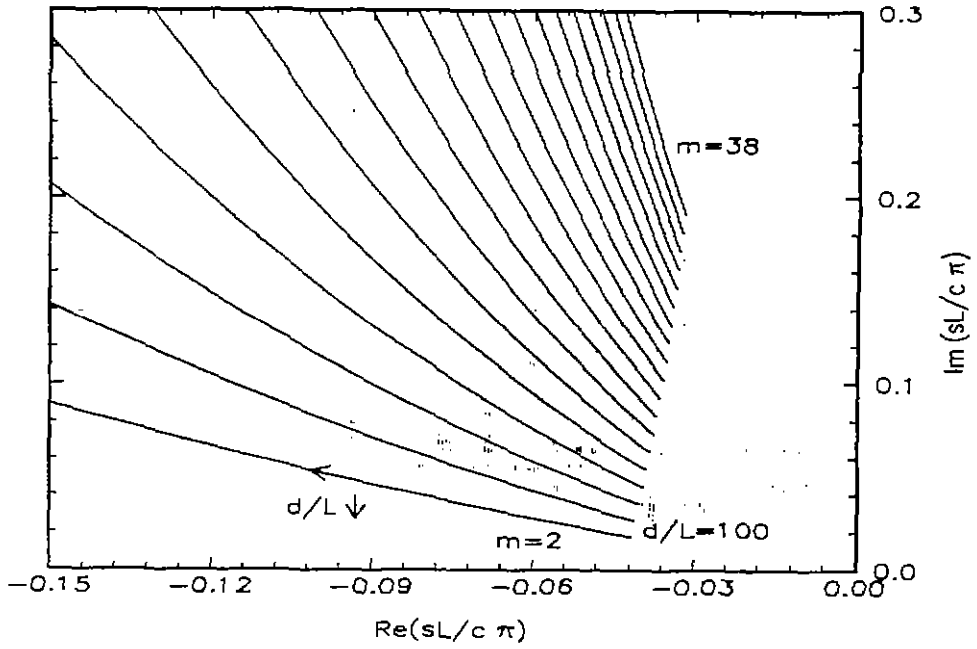

Fig. 9. Portion of trajectories of modes m=2 through m=38 parameterized by separation distance. Curves start at d/L=100 with separation decreasing in the direction of the arrow.

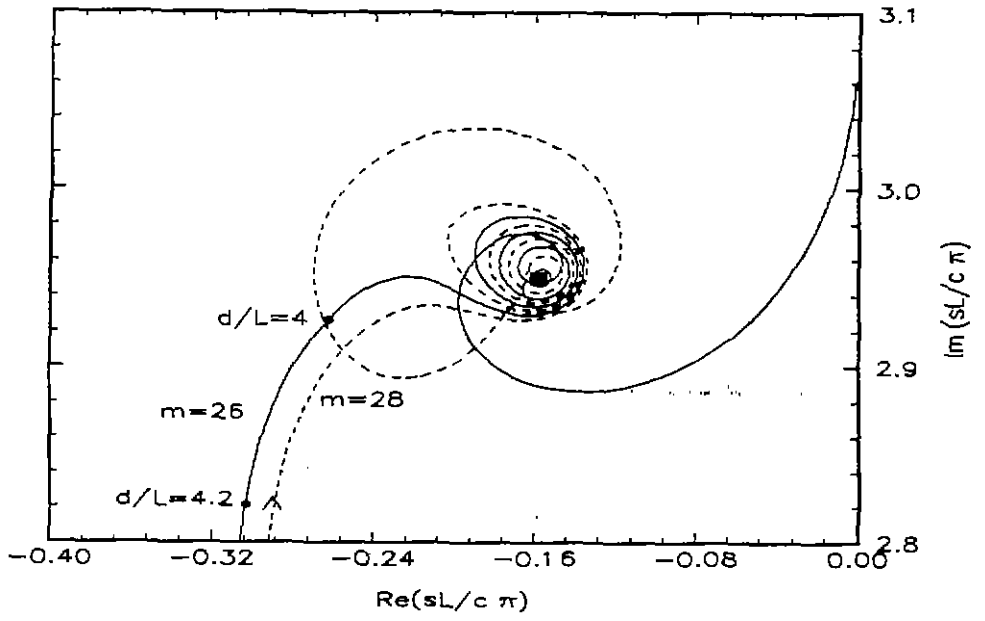

Fig. 10. Trajectories of modes m=26 (antisymmetric) and m=28 (symmetric) for small d/L values, as d/L tends towards zero, IE solution. Solid box is the location of the second (first layer) isolated-wire natural frequency.

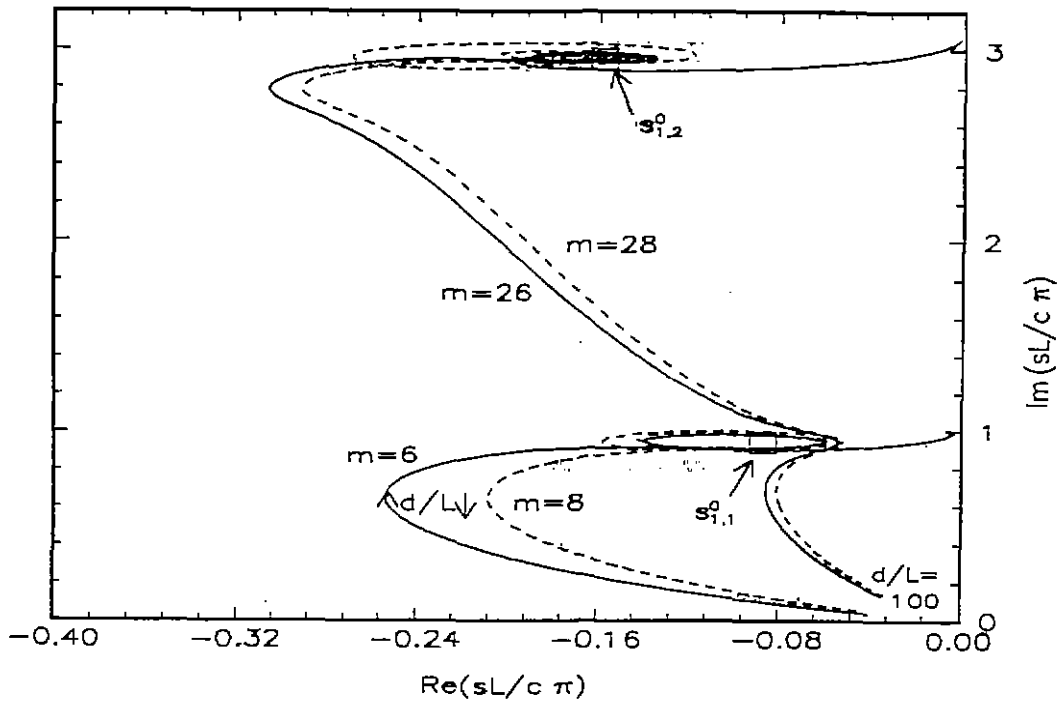

Fig. 11 Trajectories of modes m=6,8,26,28. Separation d/L varies from 100 to 0.01, IE solution.

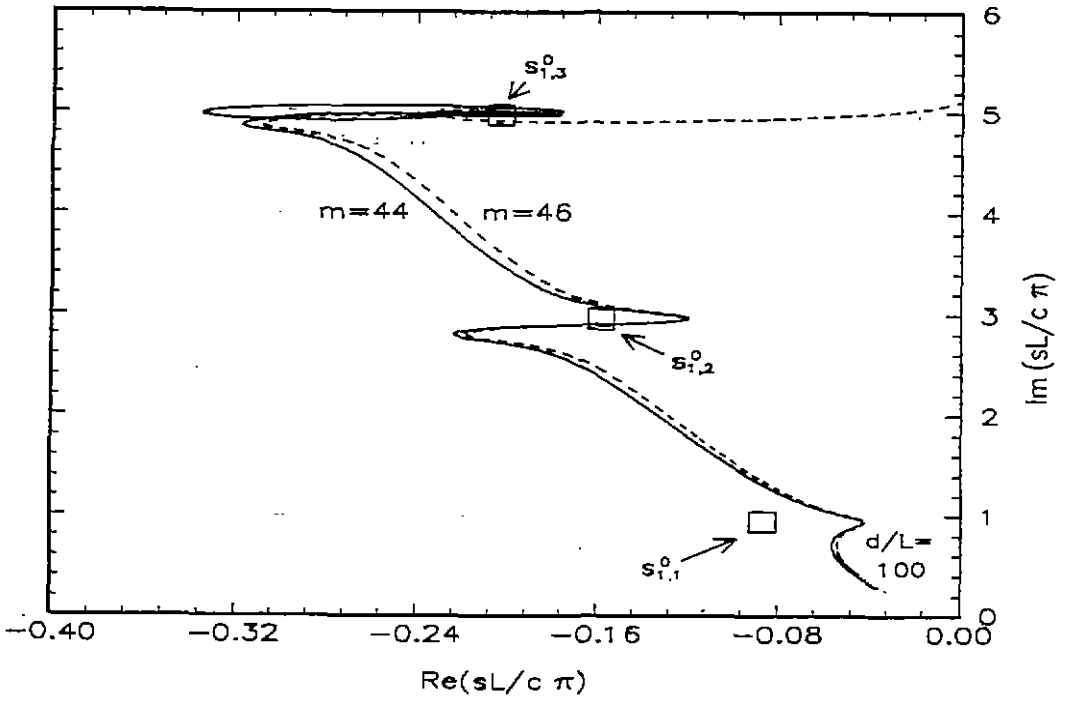

Fig. 12. Trajectories of m=44 (symmetric) and m=46 (antisymmetric) modes from d/L=100 to d/L=0.01, IE solution.

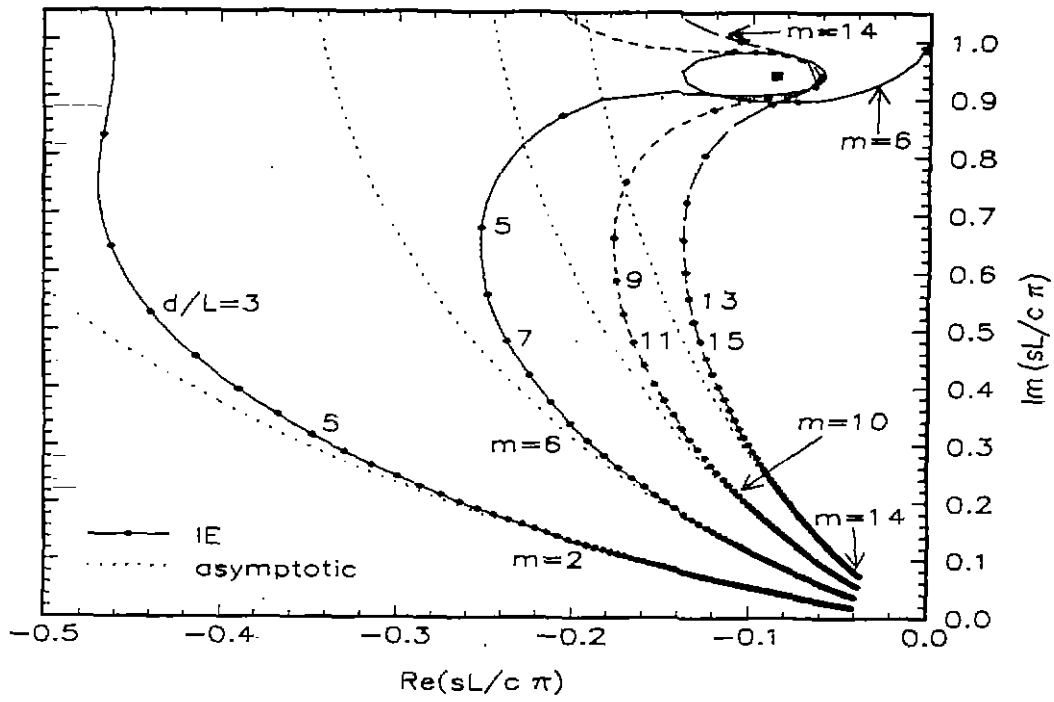

Fig. 13. Trajectory of the first four anti-symmetric modes m=2,6,10,14 of two identical parallel wires parameterized by separation distance, starting at d/L=100.

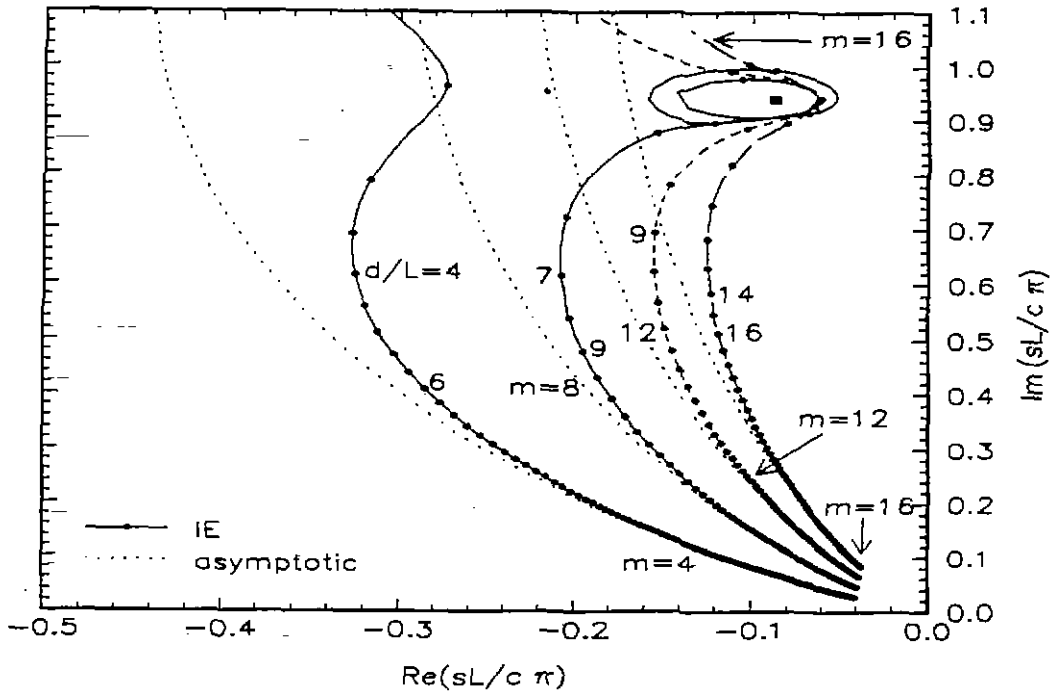

Fig. 14. Trajectory of the first four symmetric modes m=4,8,12,16 of two identical parallel wires parameterized by separation distance, starting at d/L=100.

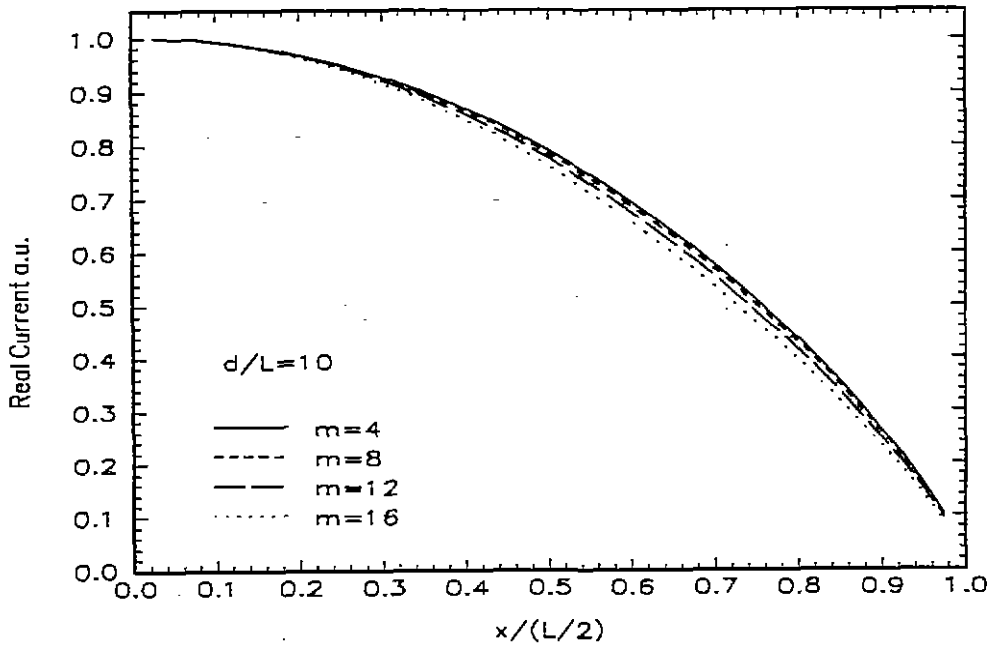

Fig. 15. Real part of symmetric natural mode current versus normalized wire length for the first four system modes at d/L=10.

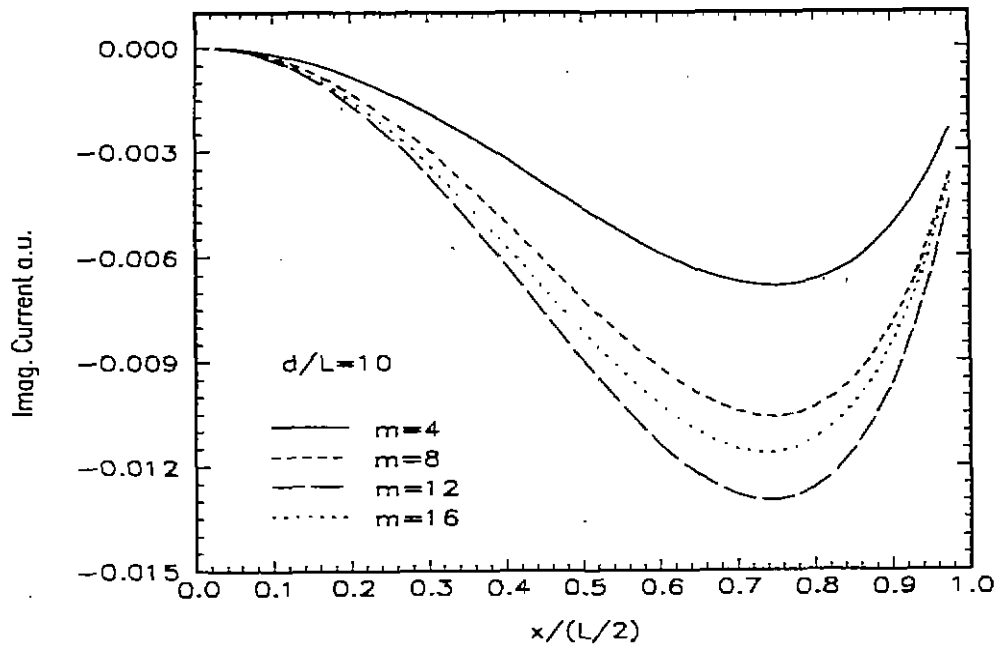

Fig. 16. Imaginary part of symmetric natural mode current versus normalized wire length for the first four system modes at d/L=10.

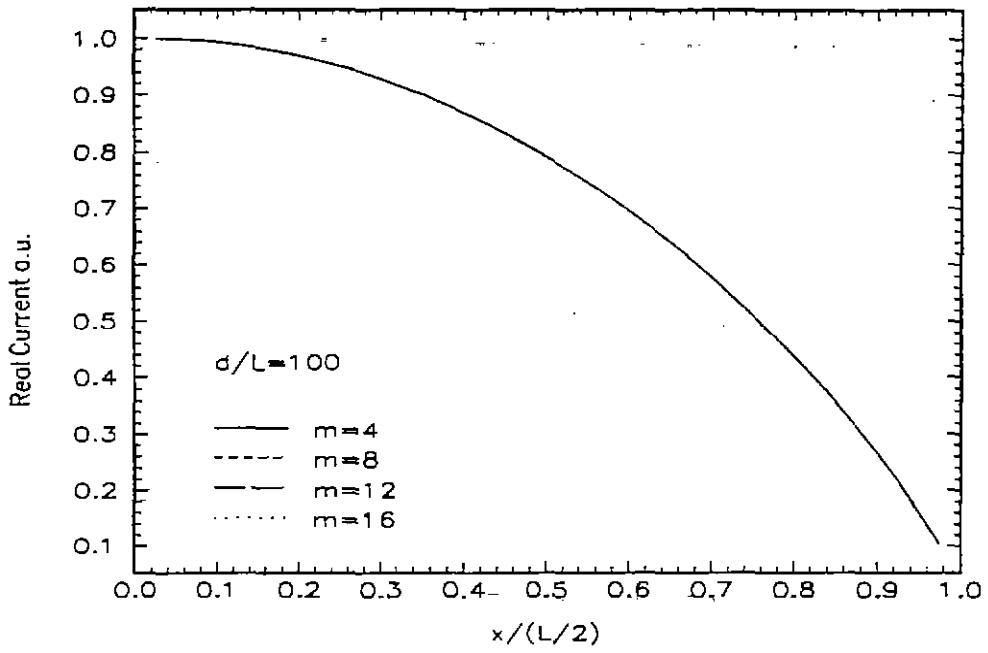

Fig. 17. Real part of symmetric natural mode current versus normalized wire length for the first four system modes at d/L=100.

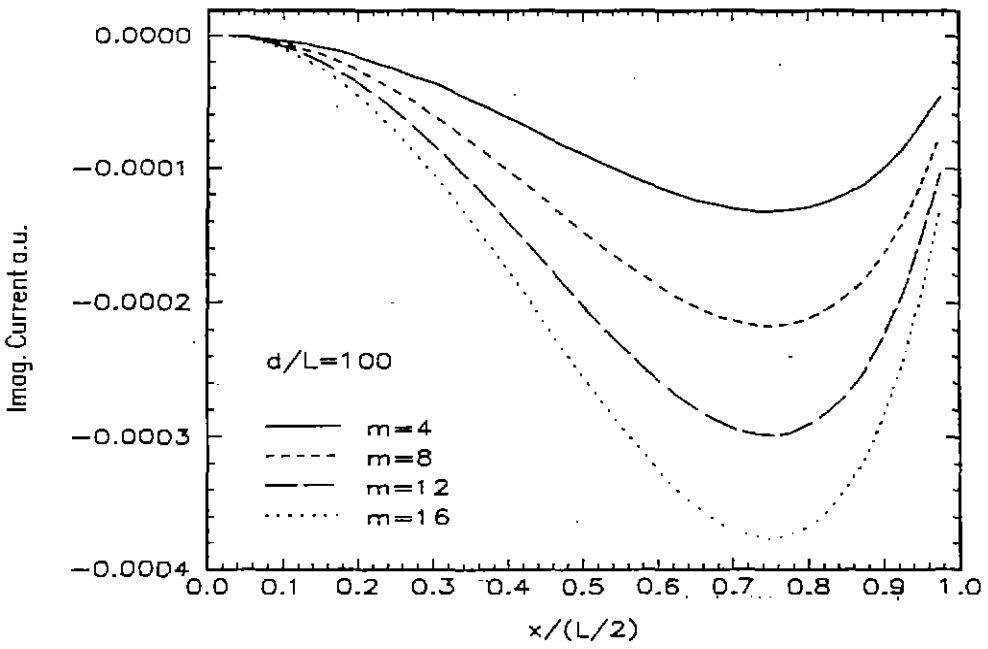

Fig. 18. Imaginary part of symmetric natural mode current versus normalized wire length for the first four system modes at d/L=100.

parallel coupled loops. Writing the equation in a general form we get

$$e^{-\Gamma}(1+\Gamma) = \mp K_z \tag{A.1}$$

where $K_z = \frac{r^3 2\pi}{P_{zz}}$ for two coupled, z-oriented wires, and $K_z = \frac{r^3 2\pi}{M_{zz}}$ for coupled loops parallel to the x-z plane. Separating Γ into real and imaginary parts as $\Gamma = \Gamma_r + j\Gamma_i$ leads to the two equations

$$\tan\Gamma_i = \frac{\Gamma_i}{1+\Gamma_r} \tag{A.2}$$

$$e^{-\Gamma_r}\left[(1+\Gamma_r)\cos\Gamma_i + \Gamma_i \sin\Gamma_i\right] = \mp K_z. \tag{A.3}$$

In Fig. A.1, the left (solid lines) and right (dashed lines) sides of (A.2) are plotted versus normalized Γ_i. Since $\Gamma_r \leq 0$ for passive media, the right-hand side of (A.2) is plotted in Fig. A.1 for several representative values of Γ_r. It can easily be seen from the figure that for a given value of Γ_r, an infinite set of intersections can be found. Since $\Gamma = \frac{s}{c} r = \gamma r$, this shows that the imaginary part of the system resonant frequency (real radian frequency) behaves as $1/r$ multiplied by a number which depends upon the specific intersection of the left and right-hand sides of (A.2).

Although (A.2) cannot be solved analytically, some general observations can be made from Fig. A.1.

(a) For $\Gamma_r = 0$, $\quad \Gamma_i \approx 0, \left\{\frac{n^- \pi}{2}, n^- = 3^-, 5^-, 7^-, \ldots\right\}$

(b) For $-1 < \Gamma_r < 0$, $\quad \Gamma_i \approx 0, \left\{\frac{n^- \pi}{2}, n^- = 3^-, 5^-, 7^-, \ldots\right\}, \left\{\frac{\alpha\pi}{2}, 0 < \alpha < 1, (\textit{one value})\right\}$

(c) For $-2 < \Gamma_r < -1$, $\quad \Gamma_i \approx 0, \left\{\frac{n^+ \pi}{2}, n^+ = 3^+, 5^+, 7^+, \ldots\right\}$

(d) For $-\infty < \Gamma_r < -2$, low order $\Gamma_i \approx 0, \left\{\frac{m^- \pi}{2}, m^- = 2^-, 4^-, 6^-, \ldots\right\}$

high order $\Gamma_i \approx \left\{\frac{n_I^+ \pi}{2}\right\}$

where n_I^+ are nonnegative odd integers. In the above, the + and - superscripts denote a number slightly greater than and less than the given integer, respectively.

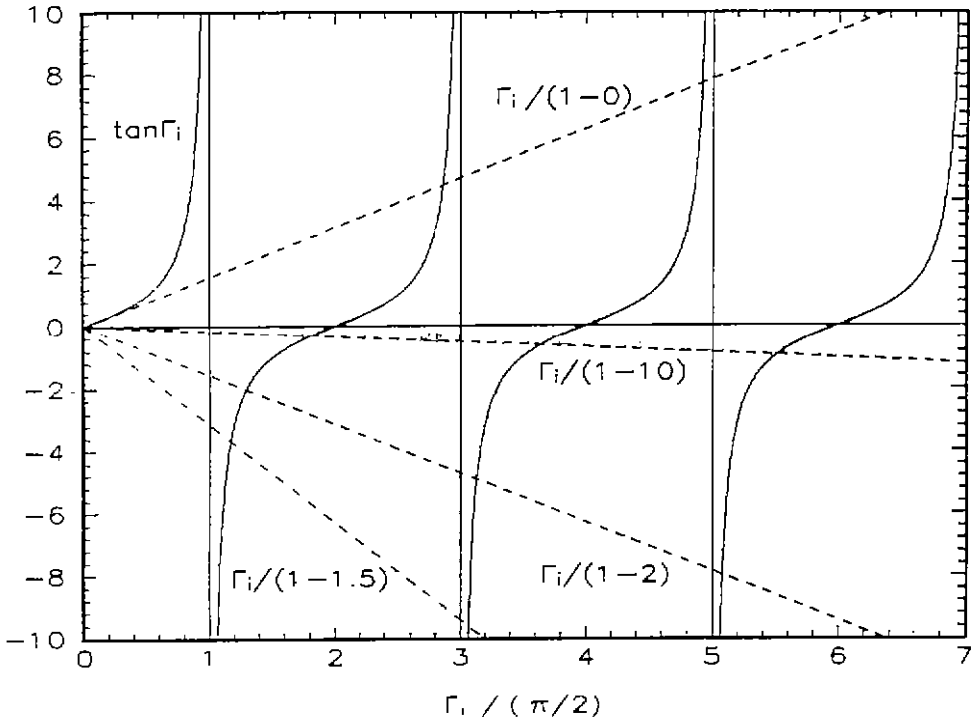

Fig. A1 Right and left-hand sides of Eq. (A2).

At this point, if one assumes that $\Gamma_i = \frac{n\pi}{2}$ for n an odd integer, (A.3) can be solved to obtain

$$\Gamma_r = \ln\left[\mp(-1)^{\frac{n-1}{2}}\frac{n\pi}{2K_z}\right]. \tag{A.4}$$

Since Γ_r is real, $\mp(-1)^{\frac{n-1}{2}} > 0$ such that the upper sign indicates $n=3,7,11,\ldots$ while the lower sign indicates $n=1,5,9,\ldots$. For the case of mirror symmetric objects, the upper sign corresponds to symmetric modes, and the lower sign to antisymmetric modes. The final expression for the approximate solution to (A.1) can be written as

$$\Gamma_n^{\binom{sy}{as}} = \ln\left[\frac{n\pi}{2K_z}\right] + j\frac{n\pi}{2} \qquad n = \begin{pmatrix}3,7,11,\ldots\\1,5,9,\ldots\end{pmatrix}. \tag{A.5}$$

The other equation of interest, (60), which arises from a study of parallel-coupled wires and parallel-coupled loops, can be written in a general form as

where $K_x = \frac{r^3 4\pi}{P_{xx}}$ (or with P_{yy}) for two parallel coupled wires and for coupled loops parallel to the x-z plane. As before, separating Γ into real and imaginary parts leads to

$$\tan\Gamma_i = \frac{\Gamma_i(1+2\Gamma_r)}{1+\Gamma_r+\Gamma_r^2-\Gamma_i^2} \tag{A.7}$$

$$e^{-\Gamma_r}\left[(1+\Gamma_r+\Gamma_r^2-\Gamma_i^2)\cos\Gamma_i+(\Gamma_i+2\Gamma_r\Gamma_i)\sin\Gamma_i\right] = \mp K_x . \tag{A.8}$$

In Fig. A.2, the left (solid lines) and right (dashed lines) sides of (A.7) are plotted versus normalized Γ_i, where the right-hand side for two values of Γ_r are shown. Although the right side of (A.7) is more complicated then that of (A.2), it can still be easily seen from the figure that for a given value of Γ_r, an infinite set of intersections can be found, showing that the real radian frequency behaves as $1/r$ multiplied by a number which depends upon the specific intersection of the left and right-hand sides of (A.7).

As with (A.2), (A.7) cannot be solved analytically, yet general observations from Fig. A.2 indicate that the high-order resonances for small Γ_r, and the low-order resonances for large Γ_r, occur approximately at $\Gamma_i \approx \frac{m\pi}{2}$, where m is a even integer. If we assume $\Gamma_i \approx \frac{m\pi}{2}$, m=2,4,6,...,

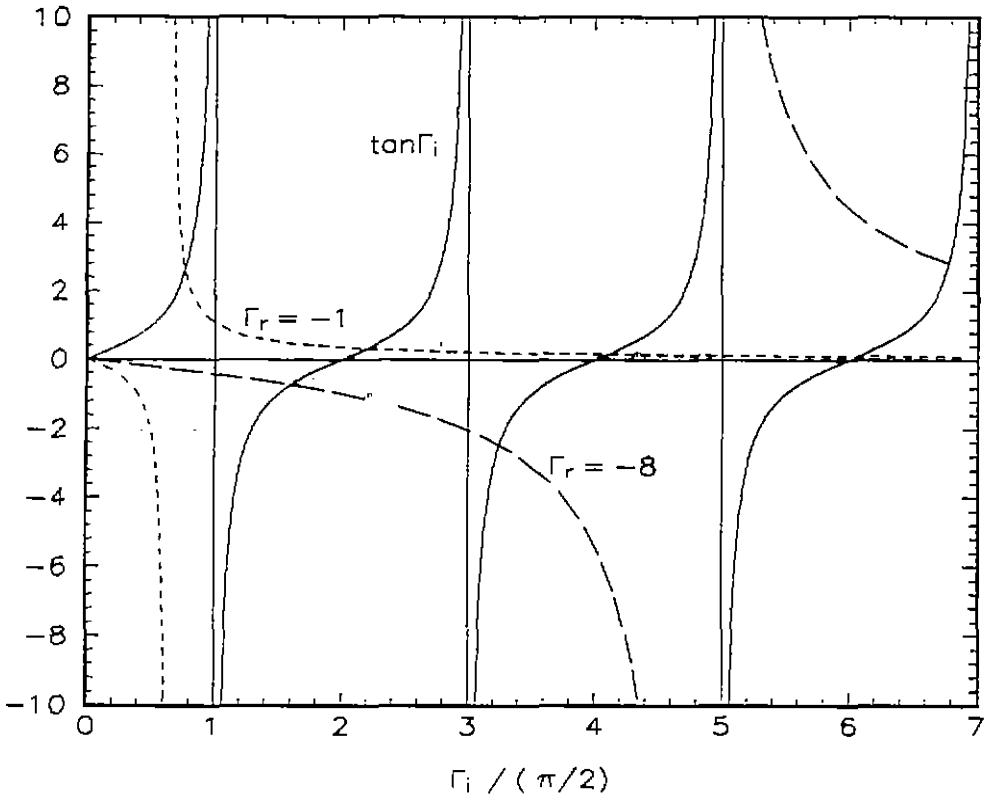

Fig. A2. Right and left-hand sides of Eq. (A7).

then (A.8) leads to

$$e^{-\Gamma_r}\left[1+\Gamma_r+\Gamma_r^2-\left(\frac{m\pi}{2}\right)^2\right](-1)^{\frac{m}{2}}=\mp K_x\,. \tag{A.9}$$

If we can further restrict our attention to high-order resonances for small Γ_r such that $\frac{m\pi}{2}>|\Gamma_r|$, (A.9) can be solved as

$$\Gamma_r=\ln\left[\pm(-1)^{\frac{m}{2}}\left(\frac{m\pi}{2}\right)^2\frac{1}{K_x}\right]. \tag{A.10}$$

Since Γ_r is real, $\pm(-1)^{\frac{m}{2}}>0$ such that the upper sign indicates $m=4,8,12,\ldots$ while the lower sign indicates $m=2,6,10,\ldots$. The final expression for the approximate solution to (A.6) can be written as

$$\Gamma_m^{(sy)}=\ln\left[\left(\frac{m\pi}{2}\right)^2\frac{1}{K_x}\right]+j\frac{m\pi}{2}\qquad m=\begin{pmatrix}4,8,12,\ldots\\2,6,10,\ldots\end{pmatrix}. \tag{A.11}$$

It should be noted that the solution (A.11) was obtained under more restrictive conditions than (A.5). Actually, (A.11) and (A.5) turn out to be quite robust formulas, in that they yield fairly accurate system frequencies upon specification of the correct value of m. Unfortunately, as can be seen from the tables, m is not actually an integer, but takes on continuous values somewhat close to the integer values obtained above. Even with the specified integer values of m, the natural frequencies provided by (A.11) and (A.5) yield sufficiently accurate numbers to use as initial guesses in a numerical solution of (A.6) and (A.1), respectively. Perhaps more importantly, the approximate solutions provide a means of classifying the modes according (approximately) to integer values of m, as discussed in Sec. VII.

The reason that the approximate solutions of the asymptotic equations are qualitatively correct and helpful for theoretical considerations, and provide reasonable numerical approximations, can be understood from Fig.s A.1 and A.2, and the form of (A.11) and (A.5). It can be seen from the figures that regardless of the value Γ_r, a discrete set of intersections between the right and left-hand sides of the plotted equations will be obtained. Thus Γ_I will be accurately described by some discrete set of values, and from the figures $\frac{m\pi}{2}$ seems a reasonable choice, with m perhaps nearly integer values for a wide range of Γ_r values. As for the real part, the logarithmic dependence on m contributes to the insensitivity of the approximate solution. For (A.11), it would be expected that the solution becomes more accurate as the condition $\frac{m\pi}{2}>|\Gamma_r|$ is satisfied, which indeed occurs as can be seen from the tables in Sec. VII.

References

[1] F.M. Tesche, "On the analysis of scattering and antenna problems using the singularity expansion technique," *IEEE Trans. Antennas Propagat.*, vol. AP-21, pp. 53-62, Jan. 1973. Also, F.M. Tesche, "On the singularity expansion method as applied to electromagnetic scattering from thin-wires," *Interaction Note 102*, April 1972.

[2] K.R. Umashankar, T.H. Shumpert, and D.R. Wilton, "Scattering by a thin wire parallel to a ground plane using the singularity expansion method," *IEEE Trans. Antennas Propagat.*, vol. AP-23, pp. 178-184, Mar. 1975.

[3] T.H. Shumpert and D.J. Galloway, "Finite length cylindrical scatterer near perfectly conducting ground. A transmission line mode approximation," *IEEE Trans. Antennas Propagat.*, vol. AP-26, pp. 145-151, Jan. 1978.

[4] L.S. Riggs and T.H. Shumpert, "Trajectories of the singularities of a thin wire scatterer parallel to a lossy ground," *IEEE Trans. Antennas Propagat.*, vol. AP-27, pp. 864-868, Nov. 1979.

[5] J.E. Ross, E.J. Rothwell, D.P. Nyquist, and K.M. Chen, "Approximate integral-operator methods for estimating the natural frequencies of coupled objects," *Radio Science*, vol. 29, pp. 677-684, 1994.

[6] C.E. Baum, T.H. Shumpert, and L.S. Riggs, "Perturbation of the SEM-pole parameters of an object by a mirror object," *Electromagnetics*, vol. 8, pp. 169-186, 1989. Also, C.E. Baum, T.H. Shumpert, and L.S. Riggs, "Perturbation of the SEM-pole parameters of an object by a mirror object," *Sensor and Simulation Note 309*, Sept. 1987.

[7] C.I. Chuang and D.P. Nyquist, "Perturbational formulation for nearly degenerate coupling," *1984 National Radio Science Meeting*, Boulder, CO., Jan. 1984.

[8] Y. Yuan and D.P. Nyquist, "Full-wave perturbation theory based upon electric field integral equation for coupled microstrip transmission lines," *IEEE Trans. Microwave Theory Tech.*, vol. 38, pp. 1576-1584, Nov. 1990.

[9] G.W. Hanson and D.P. Nyquist, "Full-wave perturbation theory for the analysis of coupled microstrip resonant structures," *IEEE Trans. Microwave Theory Tech.*, vol. 40, pp. 1774-1779, Sept. 1992.

[10] J. Van Bladel, *Singular Electromagnetic Fields and Sources*, Oxford Univ. Press, New York, 1991.

[11] A.D. Yaghjian, "Electric dyadic Green's functions in the source region," *Proc. IEEE*, vol. 68, pp. 248-263, Feb. 1980.

[12] C.E. Baum, "Some characteristics of electric and magnetic dipole antennas for radiating transient pulses, " *Sensor and Simulation Note 125*, Jan., 1971.

[13] C.E. Baum, T.K. Liu, and F.M. Tesche, "On the analysis of general multiconductor transmission-line networks, " *Interaction Note 350*, Nov, 1978.

[14] K.S.H. Lee, "Electrically-small ellipsoidal antennas, " *Sensor and Simulation Note 193*, Feb., 1974.

[15] C.E. Baum, "Interaction of electromagnetic fields with an object which has an electromagnetic symmetry plane, " *Interaction Note 63*, Mar., 1971. Also, C.E. Baum and H.N. Kritikos (Ed.s), *Electromagnetic Symmetry*, Talyor & Francis, Wash. DC, 1995.

[16] K.S.H. Lee (ed.), *EMP Interaction: Principles, Techniques, and Reference Data*, Hemisphere (Tayler & Francis), 1986.

[17] J.E. Ross, private communication.